

NAVAL POSTGRADUATE SCHOOL MONTEREY, CALIFORNIA



THESIS

**A STUDY OF FAILURE IN CARBON/FOAM
SANDWICH COMPOSITES WITH STRESS
CONCENTRATION**

by

Peter J. Sistare

September 1995

Thesis Advisor:

Young W. Kwon

Approved for public release; distribution is unlimited

DTIC QUALITY INSPECTED 3

19960215 006

REPORT DOCUMENTATION PAGE			Form Approved OMB No. 0704-0188	
Public reporting burden for this collection of information is estimated to average 1 hour per response, including the time for reviewing instruction, searching existing data sources, gathering and maintaining the data needed, and completing and reviewing the collection of information. Send comments regarding this burden estimate or any other aspect of this collection of information, including suggestions for reducing this burden, to Washington Headquarters Services, Directorate for Information Operations and Reports, 1215 Jefferson Davis Highway, Suite 1204, Arlington, VA 22202-4302, and to the Office of Management and Budget, Paperwork Reduction Project (0704-0188) Washington DC 20503.				
1. AGENCY USE ONLY (Leave blank)	2. REPORT DATE September 1995	3. REPORT TYPE AND DATES COVERED Master's Thesis		
4. TITLE AND SUBTITLE A STUDY OF FAILURE IN CARBON/FOAM SANDWICH COMPOSITES WITH STRESS CONCENTRATION		5. FUNDING NUMBERS		
6. AUTHOR(S): Sistare, Peter J.				
7. PERFORMING ORGANIZATION NAME(S) AND ADDRESS(ES) Naval Postgraduate School Monterey, CA 93943-5000		8. PERFORMING ORGANIZATION REPORT NUMBER		
9. SPONSORING/MONITORING AGENCY NAME(S) AND ADDRESS(ES)		10. SPONSORING/MONITORING AGENCY REPORT NUMBER		
11. SUPPLEMENTARY NOTES The views expressed in this thesis are those of the author and do not reflect the official policy or position of the Department of Defense or the U.S. Government.				
12a. DISTRIBUTION/AVAILABILITY STATEMENT Approved for public release; distribution is unlimited.		12b. DISTRIBUTION CODE		
13. ABSTRACT (maximum 200 words) Both experimental and numerical studies were performed to understand the failure mechanism of carbon/foam sandwich composite plates with stress concentration. The plates had circular holes and were subjected to bending and compressive loading. Both three-point and four-point bending tests were conducted. For the testing, the foam thickness, the size of the hole, the number of holes, and the hole location were varied. In addition, a finite element analysis was conducted to verify and understand the experimental results. It was found that four-point bending is not an effective test method to evaluate the effects of stress concentration at a hole. Compressive loading is an effective method. A sample without a hole fails at the quarter point due to foam core shear failure. With a hole at the center, the core shear stress at the quarter point increases with increasing hole size. However, the skin bending stress at the hole increases at a faster rate. When the hole size reaches a critical diameter, the failure mode changes to skin bending failure at the hole.				
14. SUBJECT TERMS Sandwich Composite, Stress Concentration, Finite Element Method		15. NUMBER OF PAGES 106		16. PRICE CODE
17. SECURITY CLASSIFICATION OF REPORT Unclassified	18. SECURITY CLASSIFICATION OF THIS PAGE Unclassified	19. SECURITY CLASSIFICATION OF ABSTRACT Unclassified	20. LIMITATION OF ABSTRACT UL	

NSN 7540-01-280-5500

Standard Form 298 (Rev. 2-89)
Prescribed by ANSI Std. Z39-18 298-102

Blank Pages

Approved for public release; distribution is unlimited.

**A STUDY OF FAILURE IN CARBON/FOAM SANDWICH
COMPOSITES WITH STRESS CONCENTRATION**

Peter J. Sistare
Lieutenant, United States Coast Guard
B.S., United States Coast Guard Academy, 1989

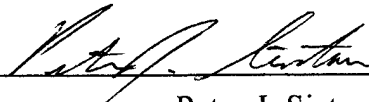
Submitted in partial fulfillment
of the requirements for the degree of

MASTER OF SCIENCE IN MECHANICAL ENGINEERING

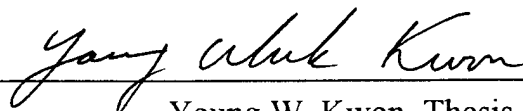
from the

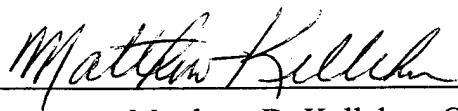
**NAVAL POSTGRADUATE SCHOOL
September 1995**

Author:


Peter J. Sistare

Approved by:


Young W. Kwon, Thesis Advisor


Matthew D. Kelleher, Chairman
Department of Mechanical Engineering

ABSTRACT

Both experimental and numerical studies were performed to understand the failure mechanism of carbon/foam sandwich composite plates with stress concentration. The plates had circular holes and were subjected to bending and compressive loading. Both three-point and four-point bending tests were conducted. For the testing, the foam thickness, the size of the hole, the number of holes, and the hole location were varied. In addition, a finite element analysis was conducted to verify and understand the experimental results. It was found that four-point bending is not an effective test method to evaluate the effects of stress concentration at a hole. Compressive loading is an effective method. A sample without a hole fails at the quarter point due to foam core shear failure. With a hole at the center, the core shear stress at the quarter point increases with increasing hole size. However, the skin bending stress at the hole increases at a faster rate. When the hole size reaches a critical diameter, the failure mode changes to skin bending failure at the hole.

TABLE OF CONTENTS

I. INTRODUCTION.....	1
II. LITERATURE SURVEY.....	3
III. EXPERIMENTAL APPARATUS.....	5
IV. BENDING TEST.....	7
A. FOUR-POINT BENDING.....	7
B. FOUR-POINT AND THREE-POINT CLASSICAL BEAM BENDING INVESTIGATION.....	8
C. FOUR-POINT AND THREE-POINT BENDING WITH LOCAL STRESS REDUCERS.....	9
D. FOUR-POINT BENDING TO FAILURE WITH LOCAL STRESS REDUCERS.....	10
V. COMPRESSION TEST.....	47
VI. COMPRESSION WITH DELAMINATION.....	75
VII. FINITE ELEMENT ANALYSIS.....	81
VIII. CONCLUSIONS AND RECOMMENDATIONS.....	93
LIST OF REFERENCES.....	95
INITIAL DISTRIBUTION LIST.....	97

I. INTRODUCTION

Sandwich composites are used in the design and construction of various components of today's modern aerospace craft. The reasons behind the selection of these materials are a high strength and stiffness to density ratio, a high resistance to corrosion, and an increased fatigue life. One drawback of this selection is the difficulty in joining components of a craft made of sandwich composites. Mechanical fastening and adhesive bonding are two methods of joining the components. Mechanical fastening allows for relatively easy component replacement. However, the use of bolts or rivets requires the sandwich composite component to be constructed with bolt/ rivet holes. The holes cause stress concentration. The stress concentration can be reduced by the use of buffer strips in the case of laminated composites and by the use of isotropic strain relief inserts in the case of laminates with a high degree of anisotropy. Stress concentration in composite materials around a hole continues to be an area under study. The objective of this study is to further understand the effects of stress concentration on foam cored sandwich composites. The study consists of experimental testing and numerical modeling of a carbon/foam sandwich composite plate with stress concentration due to a circular hole. The plates were subjected to four-point bending, three-point bending, and compressive loading. Foam thickness, hole size, hole location, and the number of holes were varied. A finite element analysis was conducted to verify and understand the experimental results.

II. LITERATURE SURVEY

Lingaiah and Suryanarayana [Ref. 1] conducted an experimental and analytical investigation of the mechanical properties of sandwich composite beams. The beams were constructed of various combinations of fiberglass reinforced plastic and aluminum skins with aluminum honeycomb or foam cores. Four-point and three-point bending tests were conducted. The experimental results showed failure at loads lower than analytically predicted failure loads. Skin-foam bond failure occurred prior to the skin reaching its ultimate tensile/ compressive strength or the foam reaching its ultimate shear stress. The authors also suggested that there was no single source that provided the mechanical properties of all skin/ core combinations of a sandwich composite. Therefore the recommendation was that sandwich structures be designed based on experimentally obtained mechanical properties rather than theoretically obtained values.

Clawson [Ref. 2] conducted an experimental investigation of the carbon skin, foam core sandwich composite. The study included impact testing of non-delaminated and delaminated samples and the subsequent residual strength of these samples to withstand a compressive load under simply supported conditions.

Prasad and Shuart [Ref. 3] derived a closed form solution to the moment distribution around a hole in a symmetric composite laminate subjected to a bending moment.

Ueng and Lin [Ref. 4] conducted a numerical study of the stress concentration caused by two identical elliptical holes in composite laminates subjected to in-plane loads and shear loads. Three orthotropic cases were studied. Hole spacing, size, and geometry were varied. It was determined that the effect of a second hole may be ignored if the distance between the hole centers is no more than three to four times the major axis of the elliptical hole.

Meyer and Dharani [Ref. 5] developed an approximate analytical model to determine the stress concentration around a hole in a buffer strip laminate. The results showed that lower modulus and higher failure strain buffer strips are most effective in increasing the strength of laminates with circular cutouts.

Franco and Cloud [Ref. 6] conducted an experimental and analytic study of stress concentration reduction near a hole in an anisotropic glass-epoxy laminate by use of isotropic strain relief inserts. The results showed that the use of stiff strain relief inserts results in the most significant stress concentration reduction.

III. EXPERIMENTAL APPARATUS

The composite beams are of sandwich construction consisting of a rohacell foam core with a thickness of 3.00 mm (0.12 in), 6.35 mm (0.25 in), or 12.70 mm (0.5 in) and two laminated carbon skins. The beam dimensions are 38.10 cm (15 in) long by 3.81 cm (1.5 in) wide. The strain gauges used were Measurements Group Inc type CEA-06-250UN, 350 ohm, gage factor 2.1. Four point bending fixtures were manufactured out of mild steel with the dimensions shown in Figure 1. The fixture contact points are 1/2" diameter steel rods. Three point bending was conducted using the bottom fixture of the four-point apparatus in conjunction with a third point centered above the beam. Column compression testing was conducted using the pinned-pinned end condition fixtures designed and manufactured as described by Clawson [Ref. 2]. The Instron Model 4507 tensile/compression test machine was used with a 200 KN load cell. Load and displacement data was obtained using the Instron Model 4500 data acquisition tower with the Instron series IX automated materials testing software, version 5.28. Strain gauge readings were acquired through the Measurements Group P-3500 strain indicator/SB-10 switch and balance unit combination.

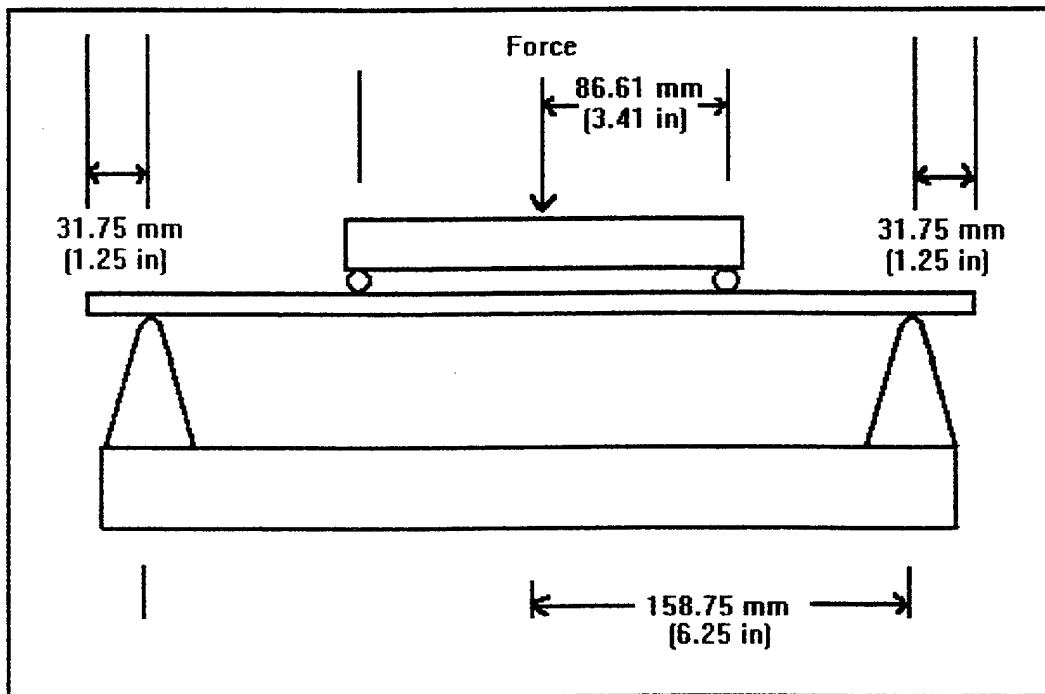


Figure 1. Four Point Bending Fixtures.

IV. BENDING TEST

Four-point and three-point bending tests were conducted to evaluate the effects of stress concentration in a foam core sandwich composite with a hole.

A. FOUR-POINT BENDING

Four-point bending tests were conducted as follows. The first beam had a 6.35 mm (0.25 in.) foam core. Two strain gauges were mounted on the sample as shown in Figure 2.

A cross head speed of 2.54 mm (0.1 in.) per minute was used for all bending tests. The specimen failed at 0.64 KN and a strain of 1350 microns. The results are shown in Figure 3 and Table 1. The point at which the load decreases is considered as the failure point. The failure occurred in the vicinity of the lower support, with delamination and foam core shear failure evident. The 1 to 1 correlation between strain gauge 1 and strain gauge 2 demonstrates symmetry of the upper and lower carbon fiber skins. One skin only will be evaluated when conducting the remaining bending tests. The deformed beam took the shape shown in Figure 4. It is uncharacteristic of classical beam bending and will be discussed further. Figure 5 shows classical beam bending. The next test was conducted under the same conditions but with a 6.35 mm (0.25 in) diameter circular hole drilled at the center of the composite strip. The hole was drilled with a backing strip to avoid delamination of the carbon skin from the foam core. One strain gauge was placed as shown in Figure 6. Failure occurred at a similar load with a higher strain. The failure however was not at the hole but at the lower support as was the case with the no-hole test. See Figure 7 and Table 2. The

deformed shape was also that of Figure 4. A third such test was conducted with a 12.70 mm (0.5 in.) diameter centered hole. The results mimicked those of the first two tests, the failure occurring at the same load and at the lower support. See Figure 8 and Table 3. The deformed beam shape remained the same as the first two tests. The results showed that stress concentration at the support was more critical than that at the hole unless the hole was very large relative to the specimen width.

B. FOUR-POINT AND THREE- POINT CLASSICAL BEAM BENDING INVESTIGATION

A sample beam was prepared with strain gauge locations as indicated in Figure 9. The beam was then subjected to four point bending and three point bending to determine if the beam deflected according to classical beam bending theory. Referring to Figure 10, classical beam bending theory stipulates that under three point bending, the strain between the lower end support and the upper point load varies linearly with the distance X between them. Similarly, referring to Figure 11, when conducting four-point bending the strain between the lower end support and the upper point load varies linearly with the distance X between them while the strain between the upper two point loads is constant. Four-point bending was conducted three times for repeatability. Strain comparisons of gauges that were not under point loads were within 3 percent when compared to the results predicted by classical beam bending. The strain comparisons between gauges located under point loads corresponded within 42 percent. See Figures 12, 13, and 14 and Tables 4, 5, and 6 respectively for the results. Next, the sample beam was subjected to three point bending within the elastic

region. Again, the test was conducted three times for repeatability. Strain measurements from gauges that were not under point loads agreed with those predicted by classical beam bending theory within 3.2 percent. The strain comparisons between gauges located under point loads corresponded within 4.0 percent. See Figures 15, 16, and 17 and Tables 7, 8, and 9 respectively for the results. The details of the six tests were reviewed to determine why the three-point bending yielded classical beam bending results while the four point bending test did not. It was noted that all load and support points were constructed of steel dowels except the upper point of the three-point bending test which was constructed of a flat plate approximately one inch wide. The results show that the strain gauges located under the dowel points produce higher strains than predicted by classical beam bending while the strain gauges under the flat plates produce strains relatively close to predicted strains. The flat plate acted to reduce the local stress concentration at the point load. Three point bending was conducted again but with the upper point constructed of a dowel. Strain comparisons of the gauge under the upper point deviated from classical beam bending by 33 Percent, up from 4.0 percent with the flat plate. The results are shown in Figure 18 and Table 10.

C. FOUR-POINT AND THREE- POINT BENDING WITH LOCAL STRESS REDUCERS

Flat plates were constructed for all load points and support points of the three and four-point bending fixtures as shown in Figures 19 and 20. The contact point plate widths were 19.05 mm (0.75 in.), 25.4 mm (1.0 in.), and 31.75 mm (1.25 in.). The sample beam was subjected to a series of three point bending tests within the elastic region utilizing the flat

plates at the upper load point and at the two support points. With the 19.05 mm (0.75 in.) plates, all strain readings correlated to predicted strains within 23 percent. When the 25.4 mm (1.0 in.) plates were used, a correlation within 15.5 percent was achieved. The 31.75 mm (1.25 in.) plates resulted in a correlation within 7.6 percent. The test results are shown in Figures 21, 22, and 23 and Tables 11, 12, and 13 respectively. The sample beam was then subjected to four-point bend testing within the elastic region, also utilizing the flat plates at the load points and at the support points. With the 25.4 mm (1.0 in.) plates, all strain readings correlated to predicted strains within 24 percent. When the 31.75 mm (1.25 in.) plates were used, a correlation within 11.82 percent was achieved. See Figures 24 and 25 and Tables 14 and 15 respectively. The data shows that the use of plates at the load point and at the support points when conducting three-point bending resulted in a correlation within 7.6 percent. A correlation within 4 percent was achieved when using a plate at the load point only. An explanation for this difference was not pursued. Three-point bending is not used to test samples with holes. Four-point bending is the test method used for this purpose. When utilized at the load points and at the support points, the plates improved the correlation for the four-point bending and were therefore implemented.

D. FOUR-POINT BENDING TO FAILURE WITH LOCAL STRESS REDUCERS

With the 31.75 mm (1.25 in.) plates acting to reduce the local stress concentrations at all four points, four-point bending was conducted on a no-hole specimen with a core thickness of 6.35 mm (0.25 in.). One strain gauge was mounted at the center of the beam. The beam failed at the lower load point and at a load similar to the failure load obtained when

testing without the plates. See Figure 26 and Table 16. The same test was conducted on a sample with a core thickness of 6.35 mm (0.25 in.) with a 12.70 mm (0.5 in) hole. The beam failed at the lower support point and at a load similar to the failure load obtained when testing this beam without the plates. See Figure 27 and Table 17. Regardless of the utilization of the flat plates, the beam failed in shear at the support point before a critical stress was reached at the hole. Although the flat plate at the support redistributes the skin bending stress around the support, it does not affect core shear stress at the support. As a result, core shear occurred at the support at the same failure load.

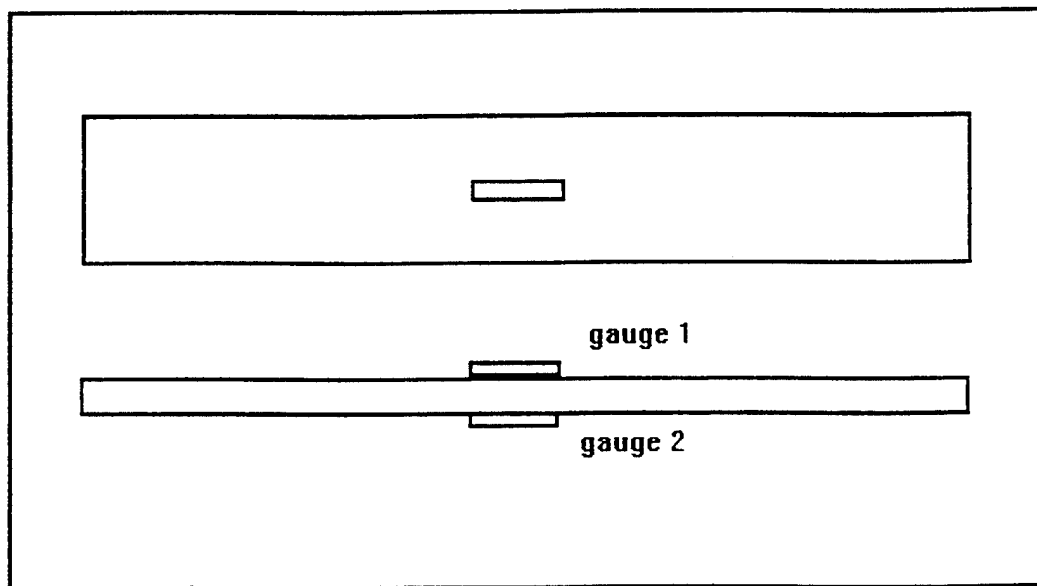


Figure 2. Strain Gauge Locations for Four Point Bending, No Hole.

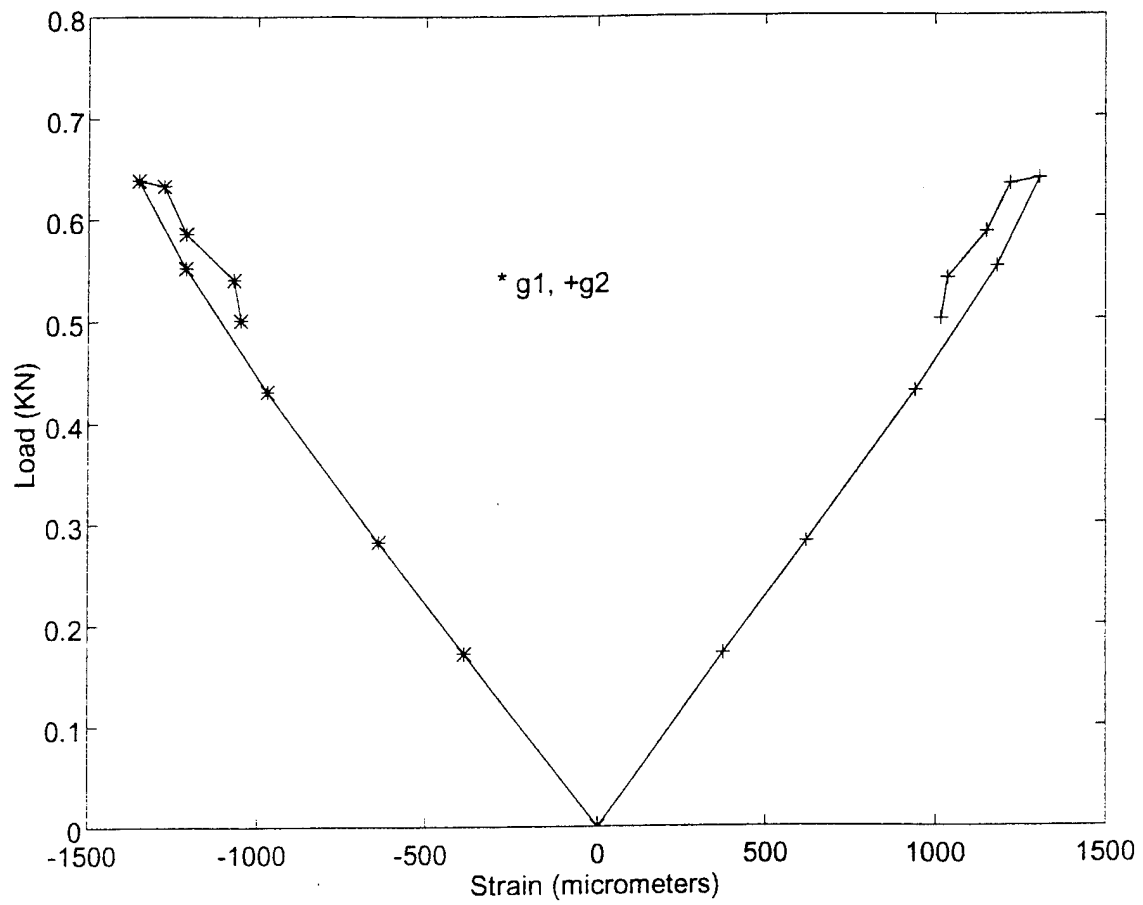


Figure 3. Load- Strain Diagram for 6.35 mm Thick, No Hole.

load (KN)	gauge1	gauge2
0.17	-384	375
0.28	-639	620
0.43	-970	943
0.55	-1212	1180
0.64	-1350	1306
0.63	-1275	1220
0.59	-1210	1150
0.54	-1070	1036
0.50	-1050	1017

Table 1. Results for Four Point Bending, No Hole.

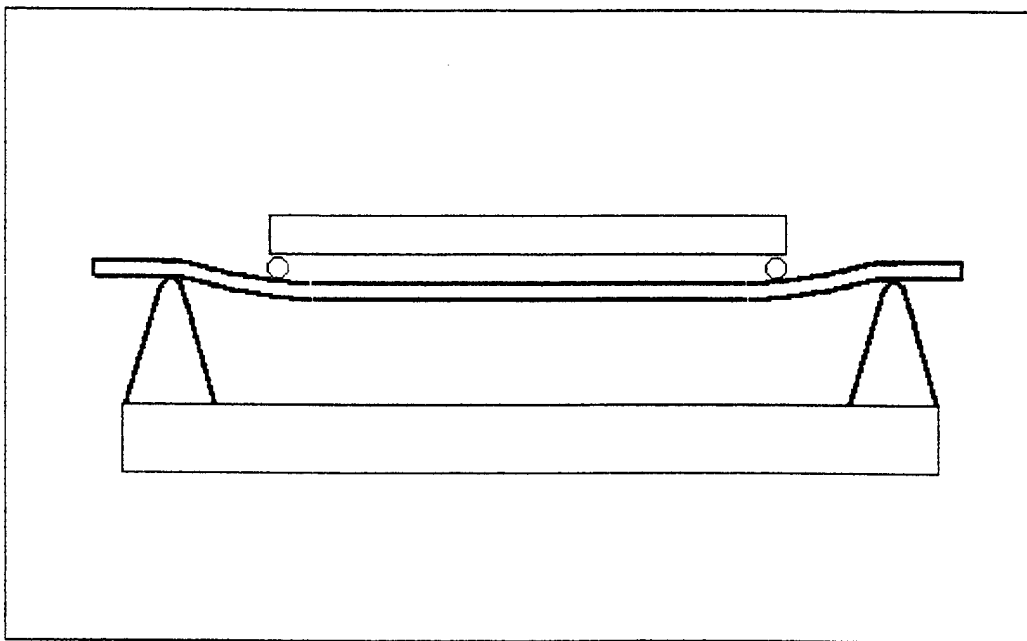


Figure 4. Bending Uncharacteristic of Classical Beam Bending Theory.

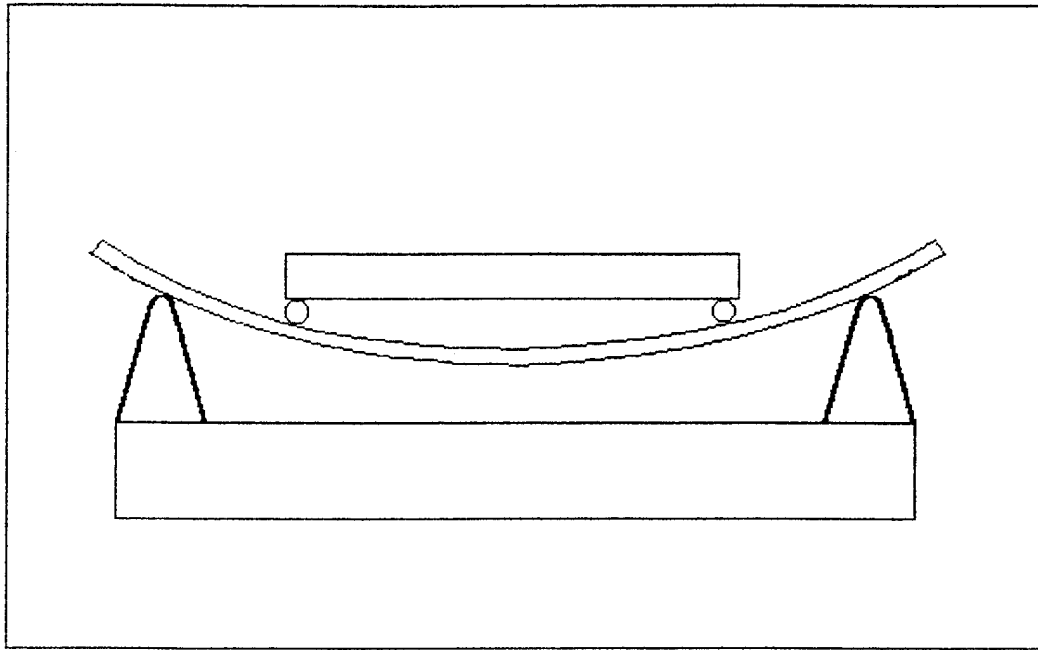


Figure 5. Bending Characteristic of Classical Beam Bending Theory.

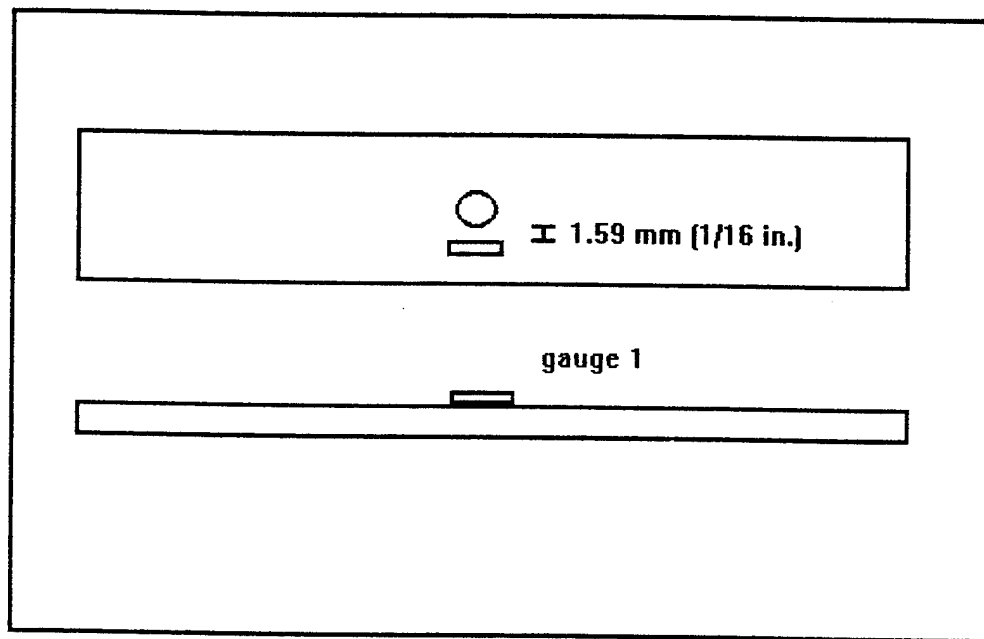


Figure 6. Strain Gauge Location for Four Point Bending, One 6.35 mm Hole.

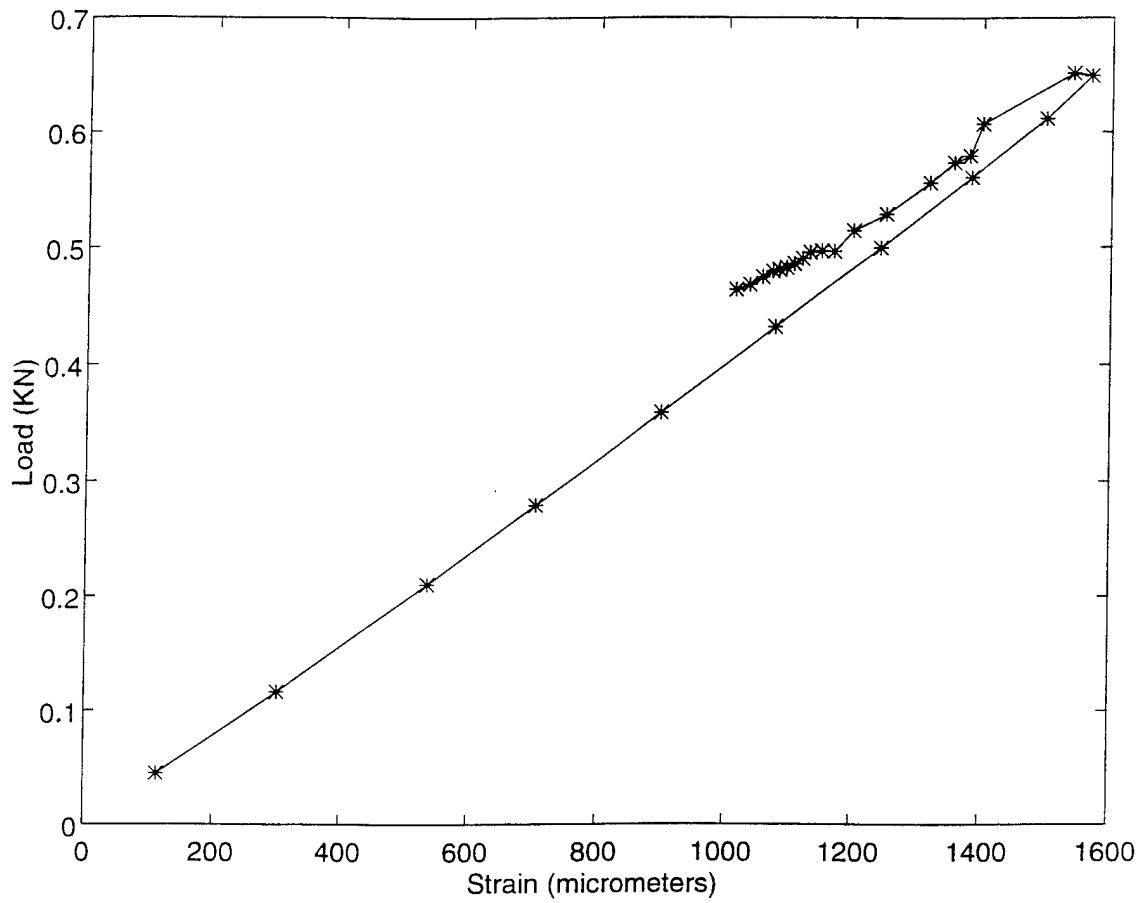


Figure 7. Load-Strain Diagram for 6.35 mm Thick, One 6.35mm Hole.

load (KN)	gauge1
0.04	113
0.12	301
0.21	536
0.28	705
0.36	901
0.43	1078
0.50	1242
0.56	1383
0.61	1499
0.65	1568
0.65	1540
0.61	1400
0.58	1380
0.57	1356
0.56	1318
0.53	1250
0.51	1200
0.50	1170
0.50	1150
0.50	1132
0.49	1120
0.49	1107
0.48	1095
0.48	1083
0.48	1073
0.48	1057
0.47	1037
0.46	1015

Table 2. Results for Four Point Bending, One 6.35 mm Hole.

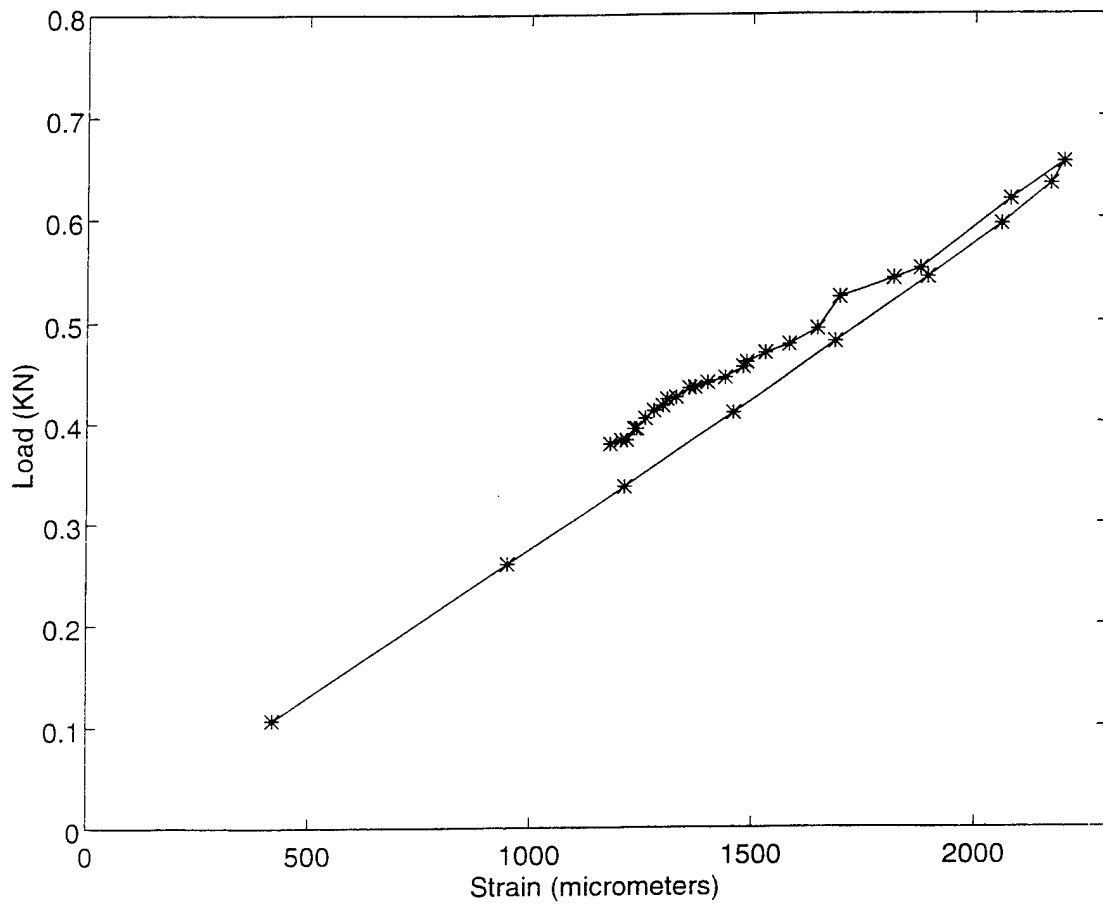


Figure 8. Load-Strain Diagram for 6.35 mm Thick, One 12.70 mm Hole.

load (KN)	gauge1
0.11	420
0.26	950
0.34	1213
0.41	1458
0.48	1690
0.54	1896
0.59	2060
0.63	2170
0.65	2200
0.62	2080
0.55	1880
0.54	1820
0.52	1700
0.49	1650
0.48	1585
0.47	1530
0.46	1488
0.46	1480
0.45	1440
0.44	1400
0.44	1372
0.44	1360
0.43	1330
0.42	1310
0.42	1300
0.41	1280
0.41	1260
0.40	1240
0.40	1235
0.38	1218
0.38	1205
0.38	1180

Table 3. Results for Four Point Bending, One 12.70 mm Hole.

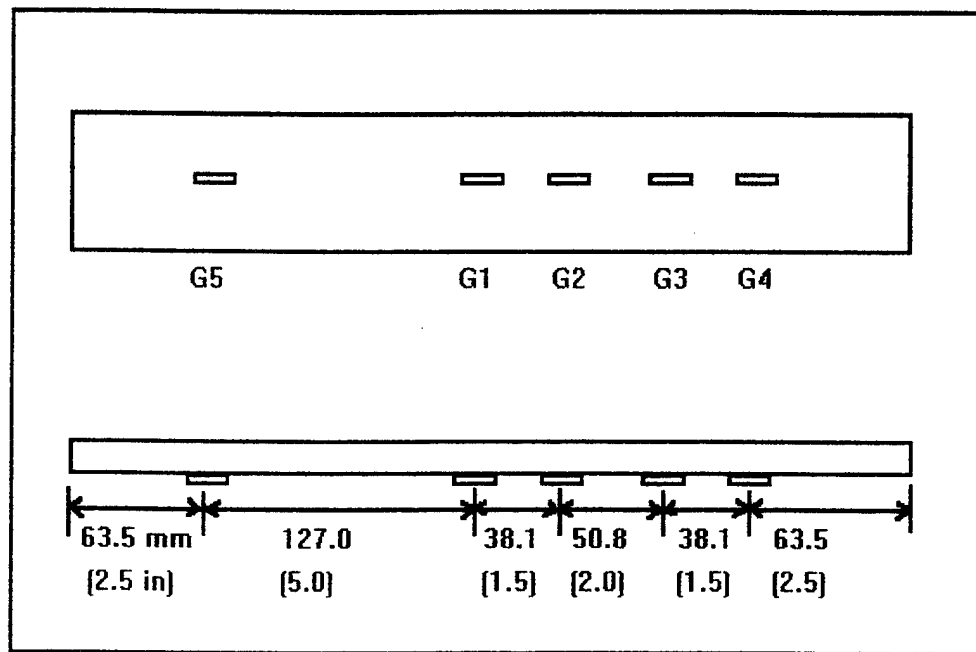


Figure 9. Strain Gauge Locations for Classical Beam Bending Investigation.

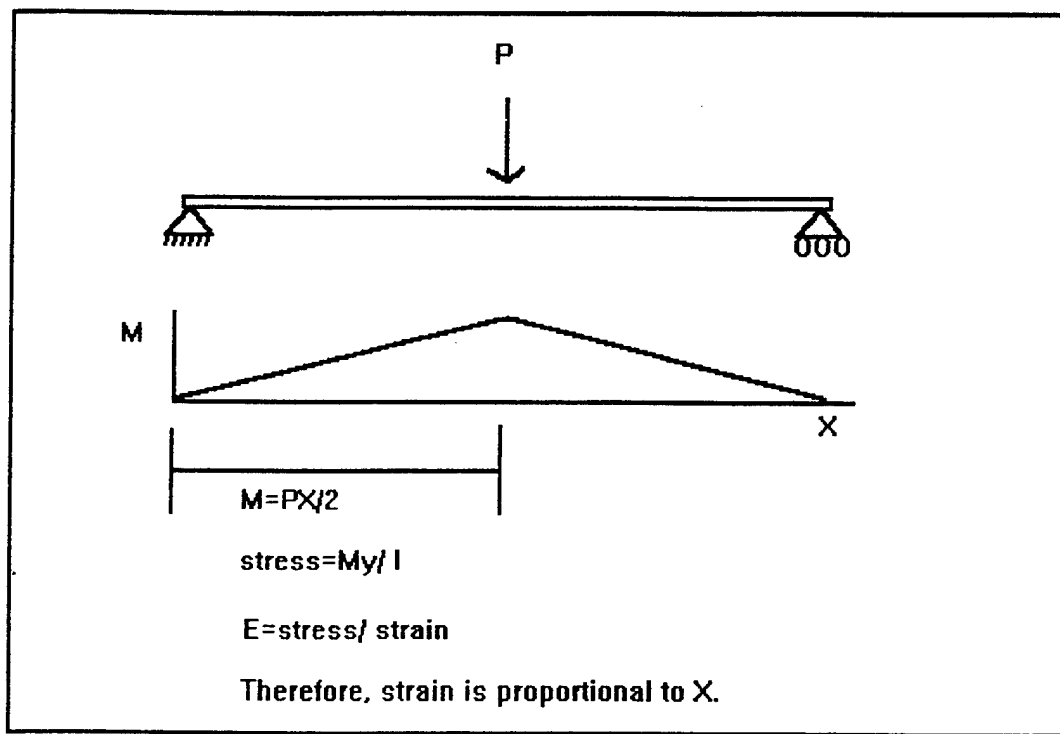


Figure 10. Classical Beam Bending Theory, Three Point Bending.

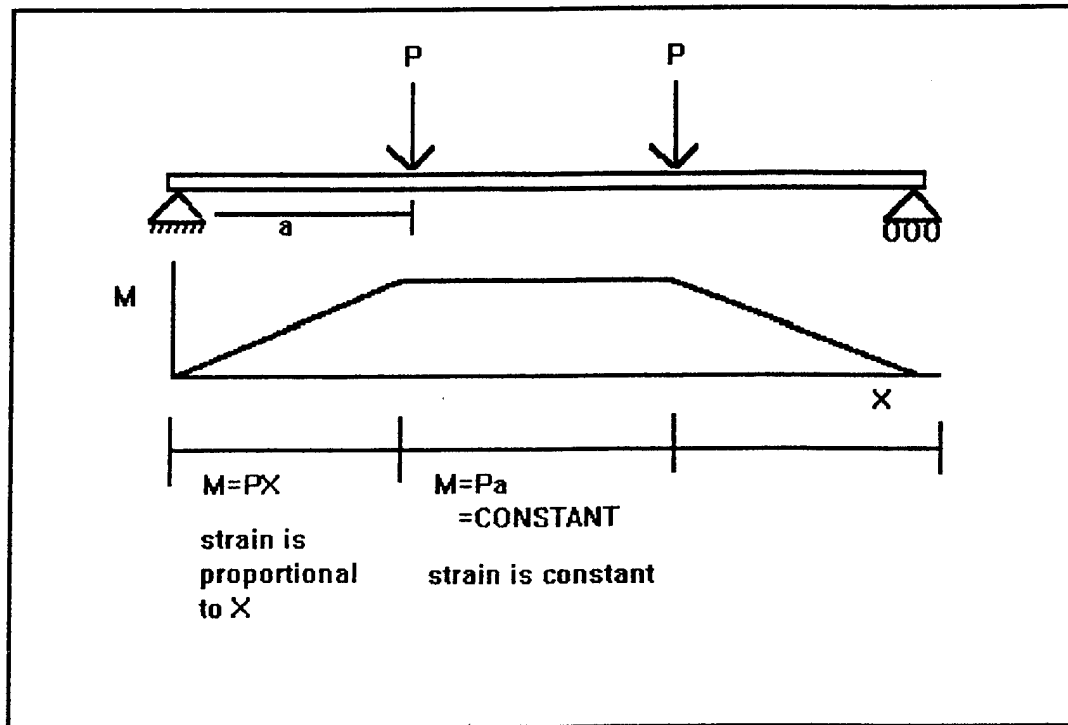


Figure 11. Classical Beam Bending Theory, Four Point Bending.

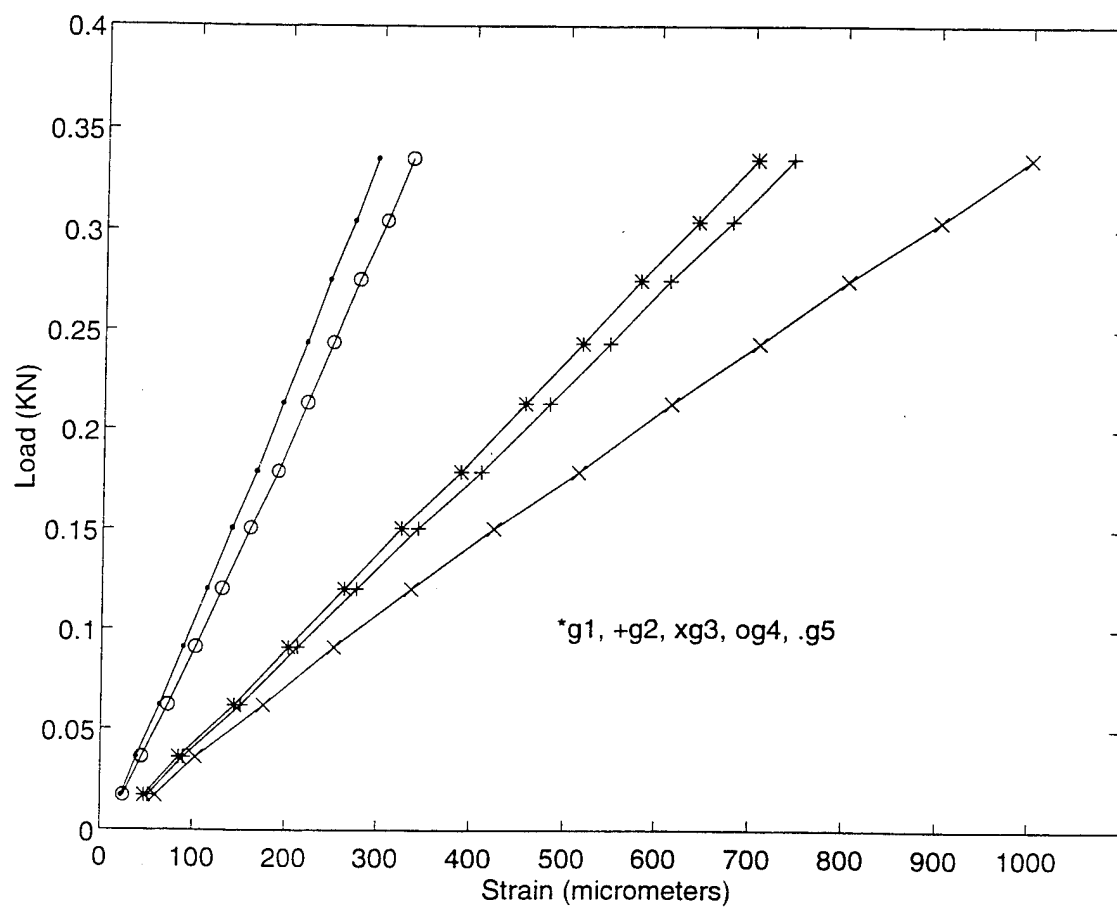


Figure 12. Classical Beam Bending Investigation, Four Point Bending Run 1.
(See Figure 9 for strain gauge locations.)

load (KN)	gauge1	gauge2	gauge3	gauge4	gauge5
0.02	48	52	60	25	23
0.04	85	90	103	45	39
0.06	144	151	176	73	64
0.09	203	213	253	102	89
0.12	264	277	336	130	114
0.15	325	343	424	160	140
0.18	388	410	514	190	166
0.21	456	482	615	221	194
0.24	517	547	708	249	22
0.28	580	612	803	277	245
0.30	642	678	901	306	271
0.34	704	743	999	333	295

Table 4. Results for Classical Beam Bending Investigation, Four Point Bending Run 1.

load (KN)	gauge1	gauge2	gauge3	gauge4	gauge5
0.01	46	50	54	24	22
0.03	89	94	105	46	41
0.06	148	156	178	74	67
0.09	212	225	265	106	93
0.12	274	290	351	134	117
0.16	349	370	458	169	147
0.19	412	438	552	199	173
0.22	476	506	651	229	199
0.25	547	582	761	262	228
0.29	612	650	863	292	255
0.32	673	714	959	320	280
0.35	738	782	1062	348	307

Table 5. Results for Classical Beam Bending Investigation, Four Point Bending Run 2.

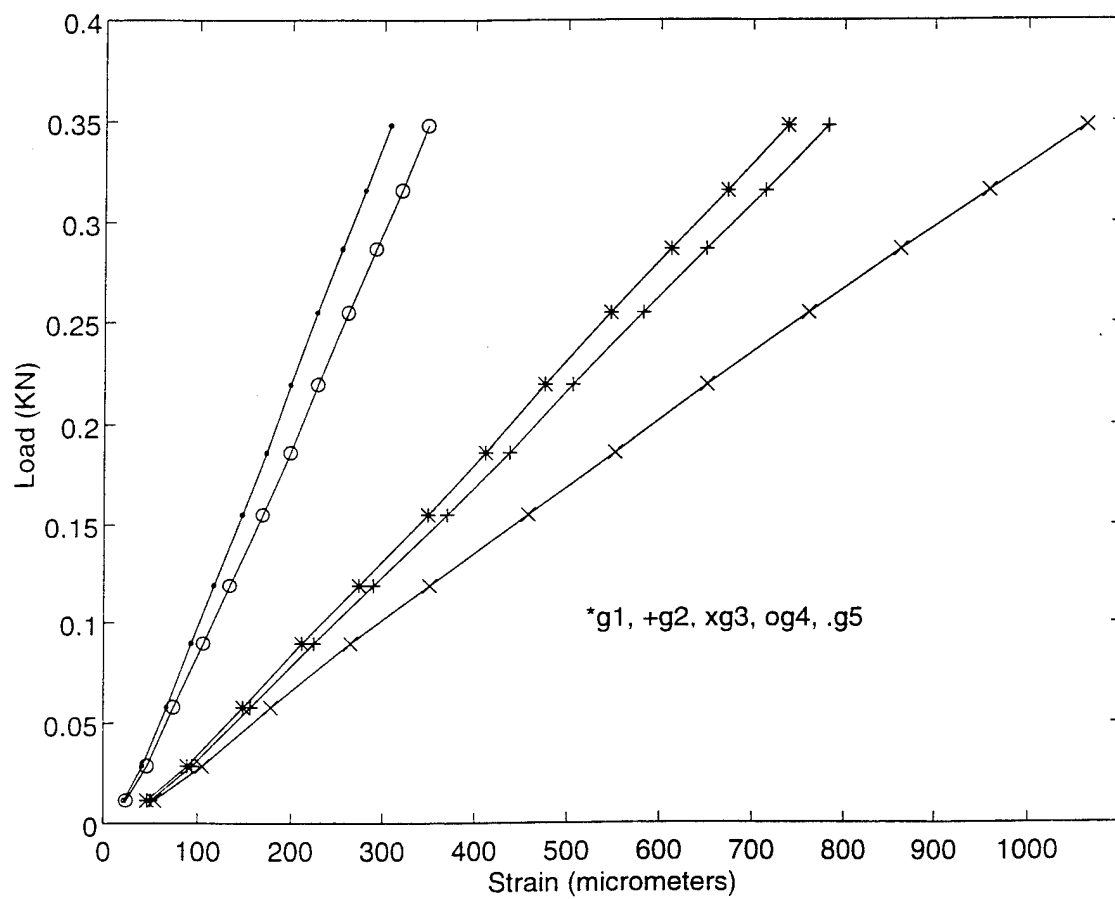


Figure 13. Classical Beam Bending Investigation, Four Point Bending Run 2.
(See Figure 9 for strain gauge locations.)

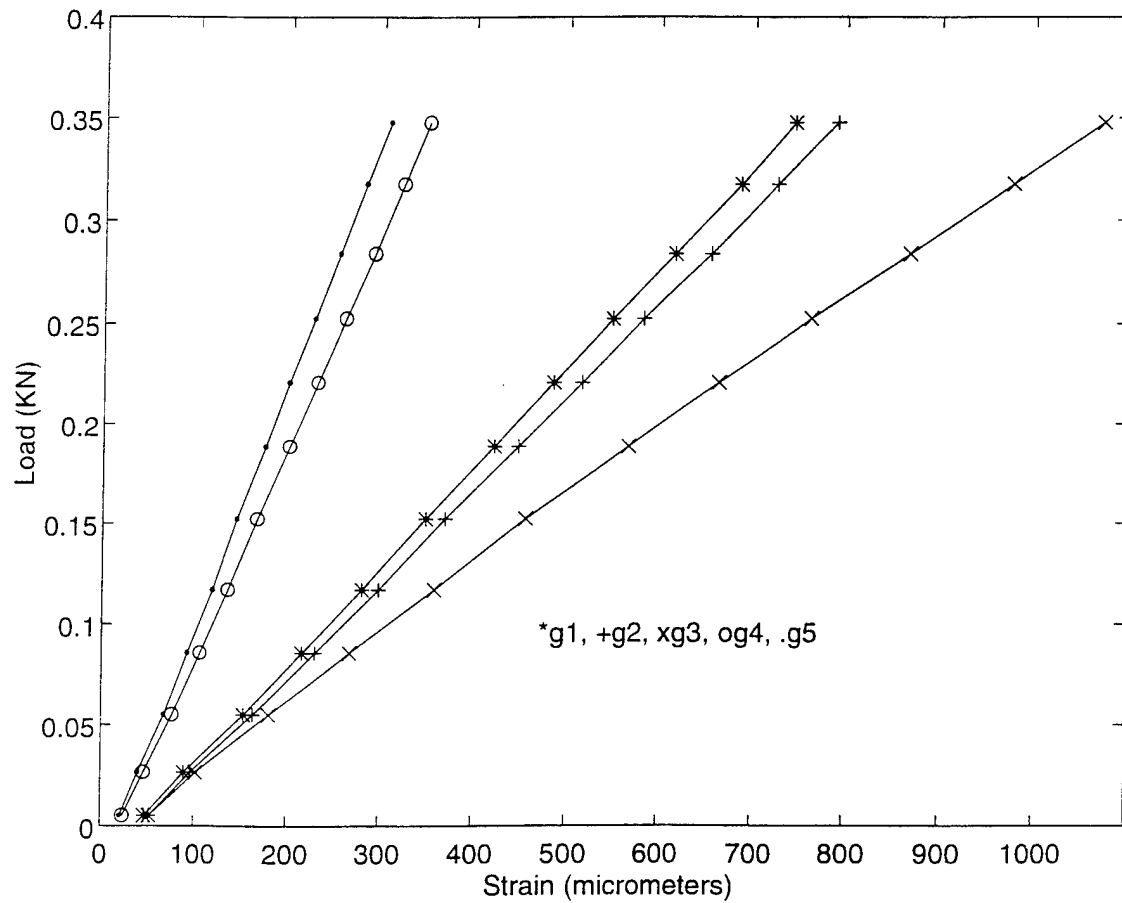


Figure 14. Classical Beam Bending Investigation, Four Point Bending Run 3.
(See Figure 9 for strain gauge locations.)

load (KN)	gauge1	gauge2	gauge3	gauge4	gauge5
0.01	47	52	52	24	21
0.03	89	96	102	46	40
0.06	154	164	181	76	67
0.09	216	230	268	106	92
0.12	281	299	359	136	119
0.15	349	370	457	167	145
0.19	423	449	567	201	175
0.22	486	516	664	231	200
0.25	549	583	764	261	227
0.28	617	655	868	292	254
0.32	686	726	977	323	282
0.35	745	791	1074	350	308

Table 6. Results for Classical Beam Bending Investigation, Four Point Bending Run 3.

load (KN)	gauge1	gauge2	gauge3	gauge4	gauge5
0.01	57	44	23	14	11
0.03	122	91	51	26	22
0.04	188	140	79	40	33
0.05	250	186	105	52	44
0.06	316	234	133	65	56
0.08	379	281	158	77	66
0.09	452	334	189	90	78
0.10	527	391	221	105	90
0.12	607	450	254	118	103
0.13	680	503	284	130	115
0.15	758	560	317	146	128
0.16	831	615	347	160	140
0.18	906	672	381	173	153
0.19	973	724	411	186	165
0.21	1044	780	442	200	178
0.22	1118	838	475	214	191
0.24	1183	888	504	227	204
0.25	1260	948	538	243	219
0.27	1331	1005	570	257	233
0.28	1401	1059	601	270	247

Table 7. Results for Classical Beam Bending Investigation, Three Point Bending Run 1.

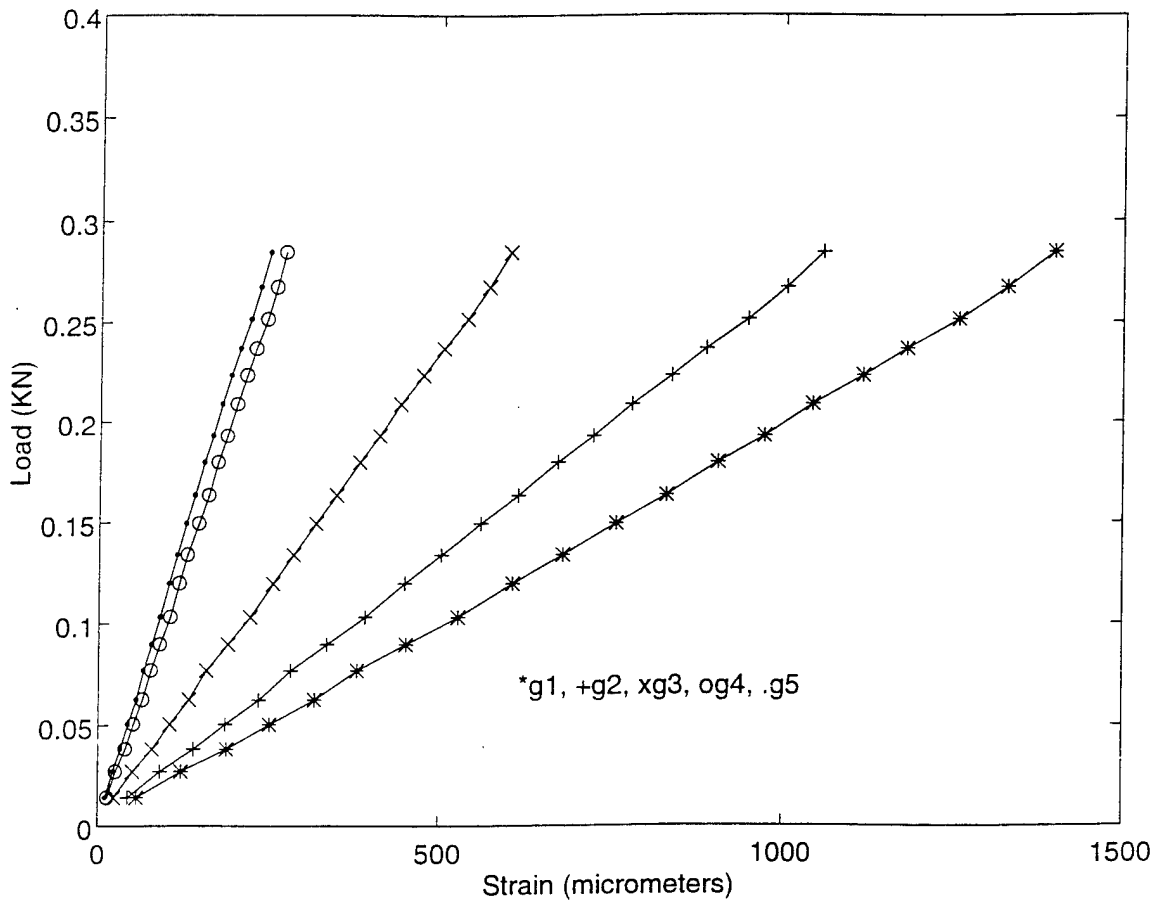


Figure 15. Classical Beam Bending Investigation, Three Point Bending Run 1.
(See Figure 9 for strain gauge locations.)

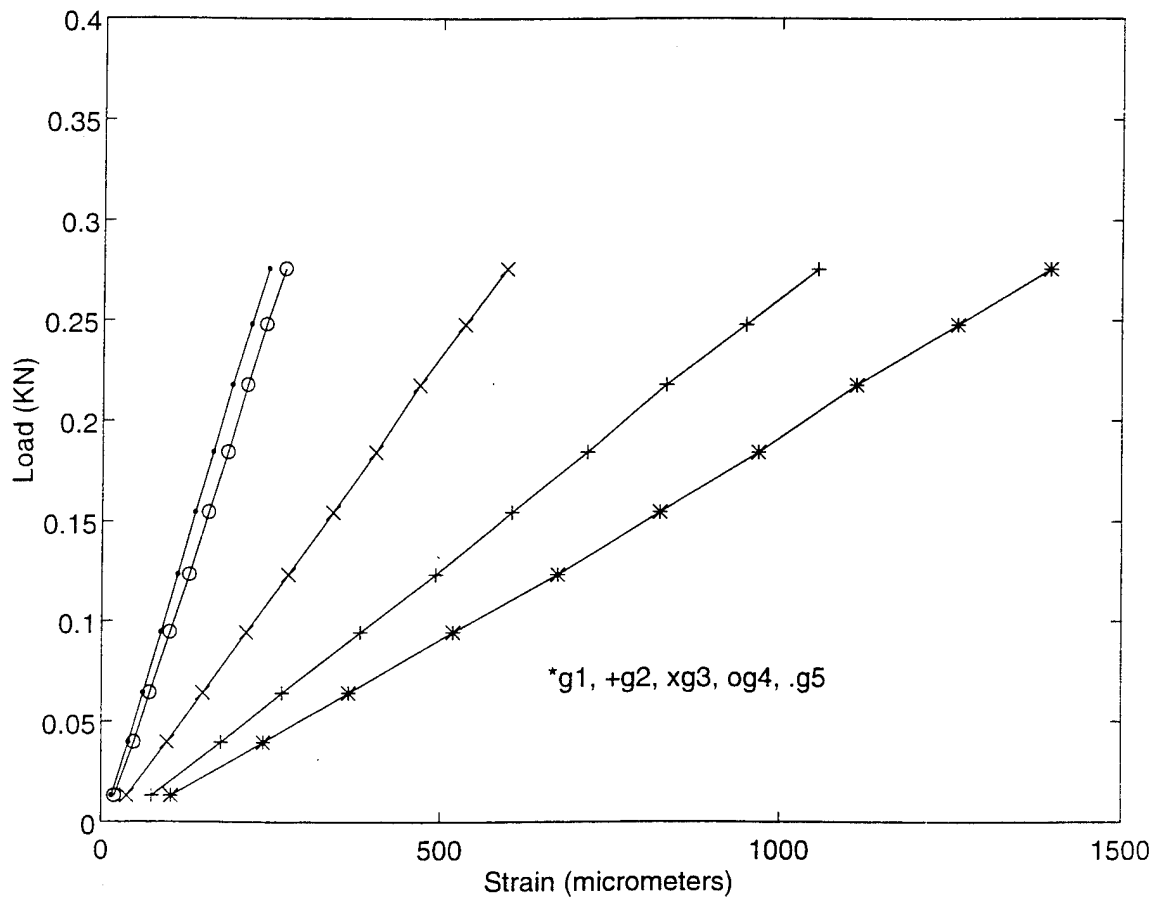


Figure 16. Classical Beam Bending Investigation, Three Point Bending Run 2.
(See Figure 9 for strain gauge locations.)

load (KN)	gauge1	gauge2	gauge3	gauge4	gauge5
0.01	101	73	37	19	15
0.04	237	174	95	47	39
0.06	363	265	147	70	60
0.09	519	380	211	99	86
0.12	673	493	274	127	110
0.15	823	605	339	155	135
0.18	968	716	402	183	161
0.22	1114	832	468	212	189
0.25	1261	949	535	240	217
0.28	1396	1056	596	268	243

Table 8. Results for Classical Beam Bending Investigation, Three Point Bending Run 2.

load (KN)	gauge1	gauge2	gauge3	gauge4	gauge5
0.01	96	68	33	17	13
0.03	232	169	91	44	37
0.06	360	263	144	69	58
0.09	515	376	208	97	83
0.12	667	487	270	124	108
0.15	824	604	337	154	134
0.18	968	717	401	181	160
0.21	1112	832	467	210	187
0.24	1260	950	534	241	216
0.28	1396	1058	594	267	242

Table 9. Results for Classical Beam Bending Investigation, Three Point Bending Run 3.

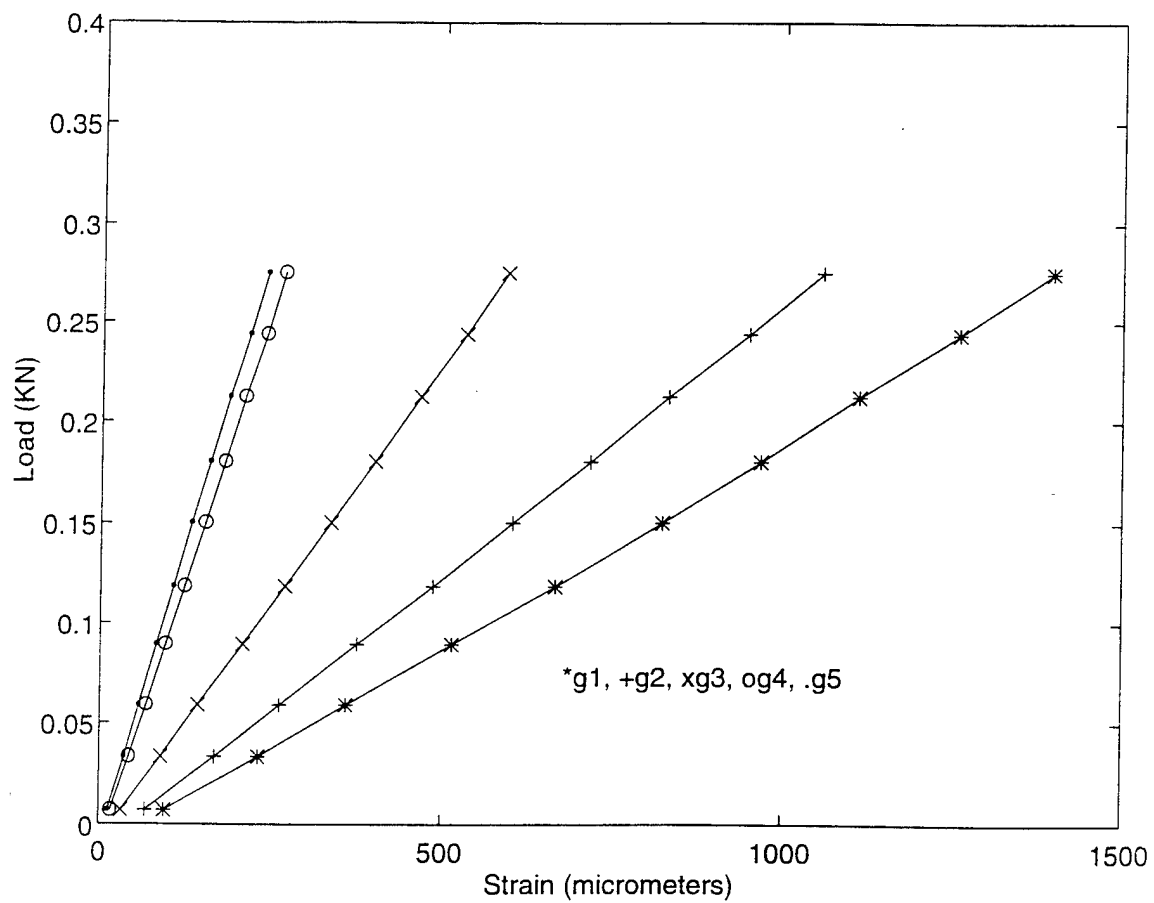


Figure 17. Classical Beam Bending Investigation, Three Point Bending Run 3.
(See Figure 9 for strain gauge locations.)

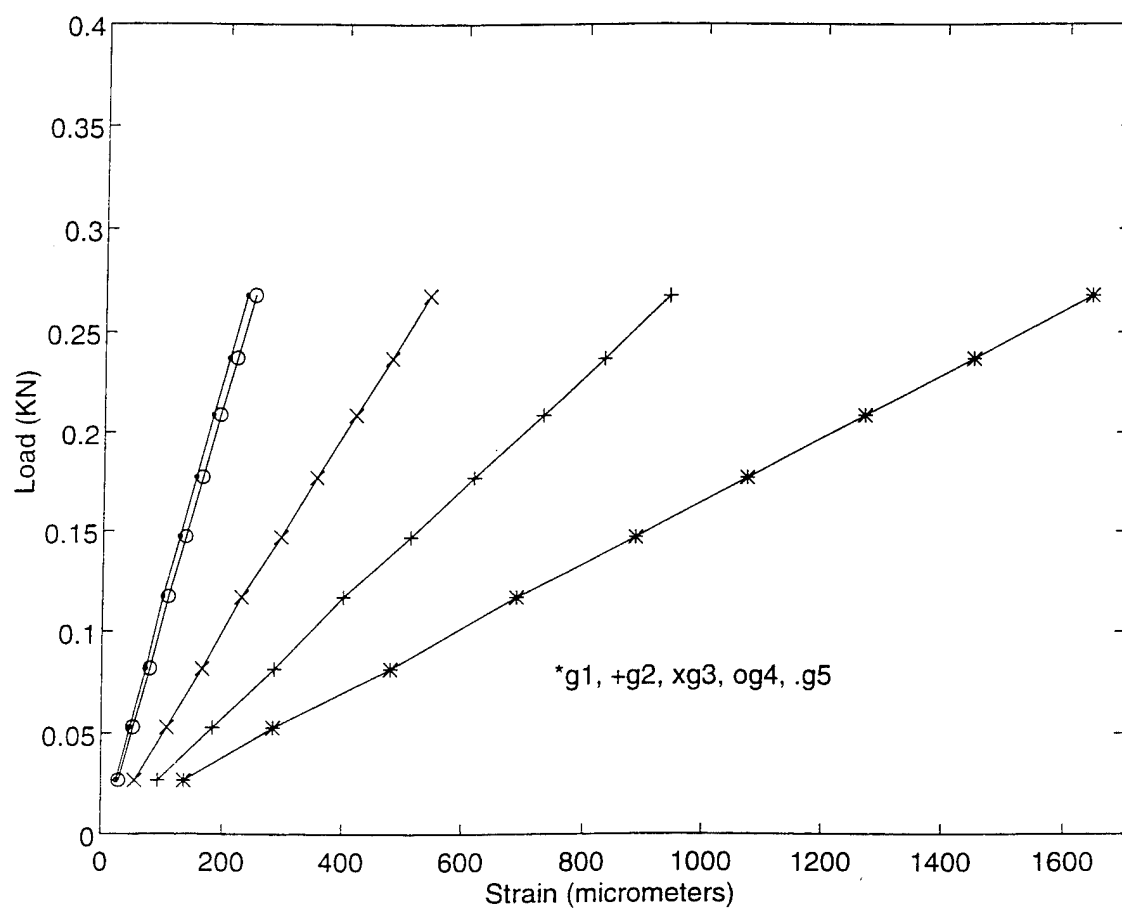


Figure 18. Three Point Bending With Flat Upper Point.
(See Figure 9 for strain gauge locations.)

load (KN)	gauge1	gauge2	gauge3	gauge4	gauge5
0.03	136	93	55	29	25
0.05	284	183	107	52	47
0.08	480	285	165	79	72
0.12	688	400	229	108	99
0.15	887	512	294	136	126
0.18	1071	617	353	163	152
0.21	1268	729	418	191	179
0.24	1449	831	478	218	205
0.27	1641	940	540	247	233

Table 10. Results for Three Point Bending with Flat Upper Point.

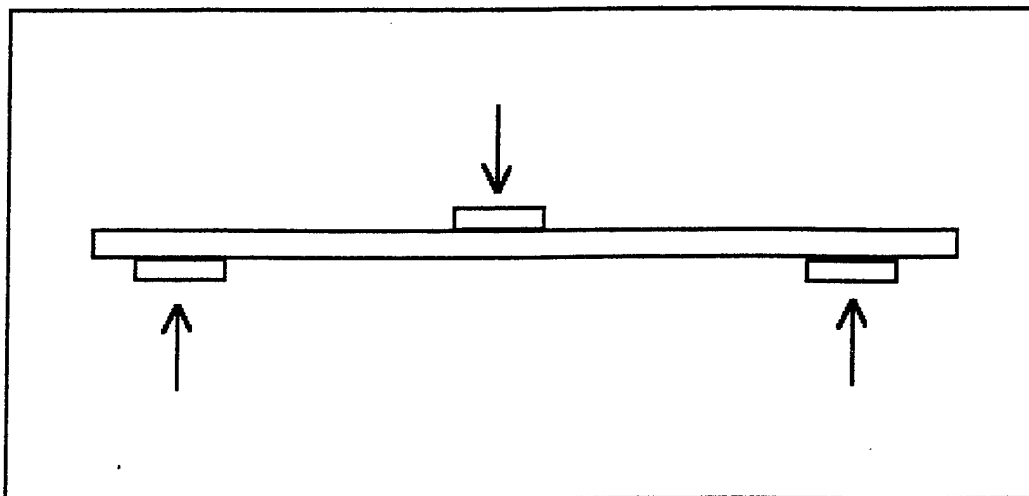


Figure 19. Local Stress Reducer Plates for Three Point Bending.

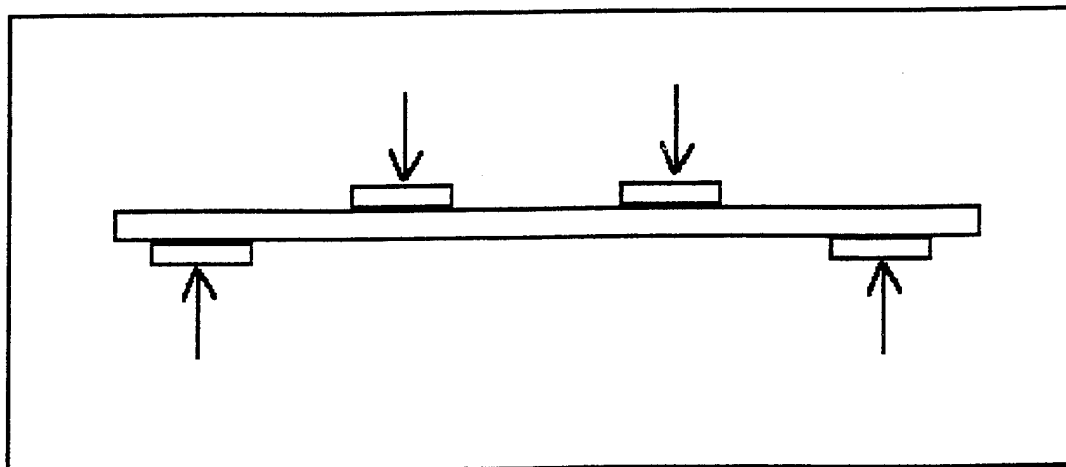


Figure 20. Local Stress Reducer Plates for Four Point Bending.

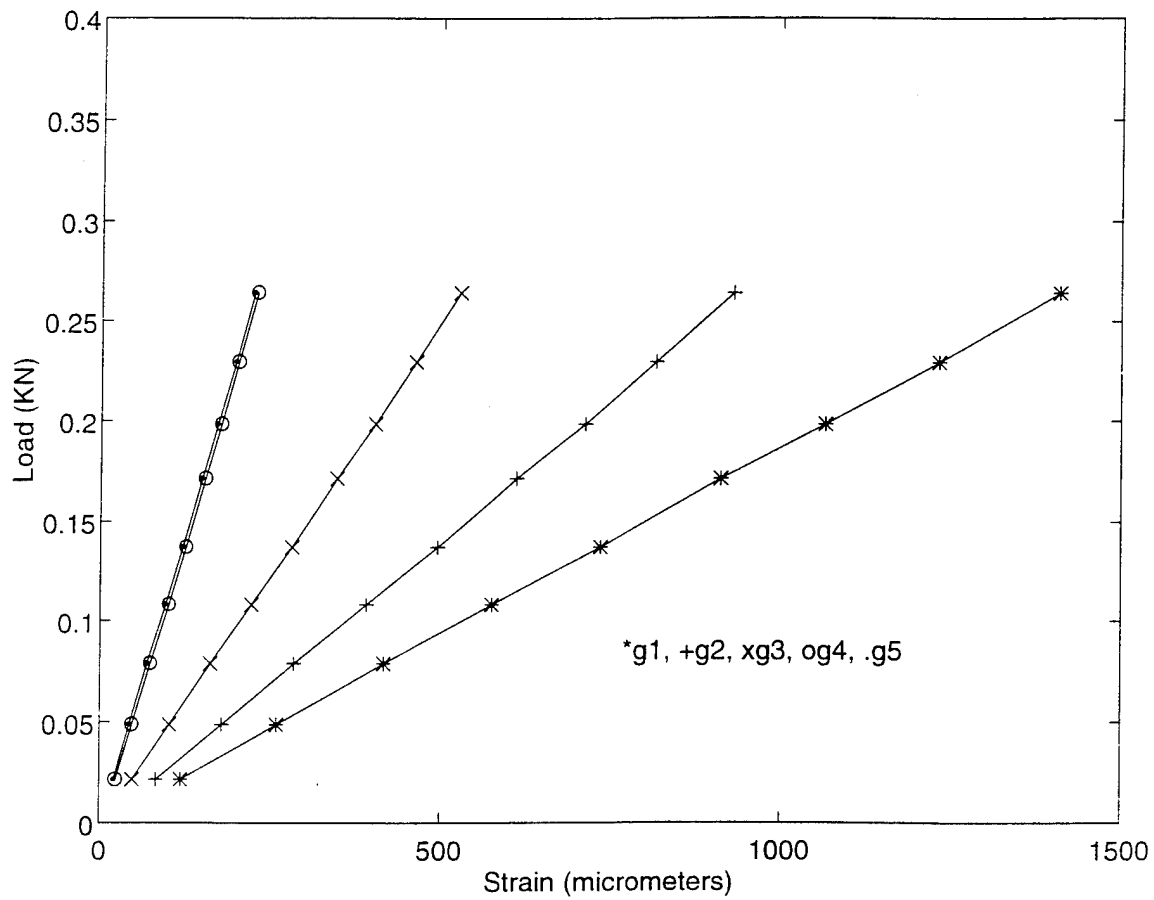


Figure 21. Three Point Bending with 19.05 mm Flat Plates.

load (KN)	gauge1	gauge2	gauge3	gauge4	gauge5
0.02	118	82	48	24	21
0.05	259	178	101	47	43
0.08	417	284	161	73	68
0.11	576	391	221	100	95
0.14	735	496	281	125	120
0.17	912	612	346	153	148
0.20	1066	712	403	176	171
0.23	1232	817	463	201	197
0.26	1410	930	528	229	224

Table 11. Results for Three Point Bending with 19.05 mm Flat Plates.

load (KN)	gauge1	gauge2	gauge3	gauge4	gauge5
0.03	114	82	48	26	23
0.05	251	178	102	51	48
0.08	397	274	158	76	73
0.11	546	385	218	103	101
0.14	702	495	279	129	129
0.17	862	604	341	155	157
0.20	1018	709	400	180	183
0.23	118	820	462	206	211
0.27	1345	930	524	233	239

Table 12. Results for Three Point Bending with 25.40 mm Flat Plates.

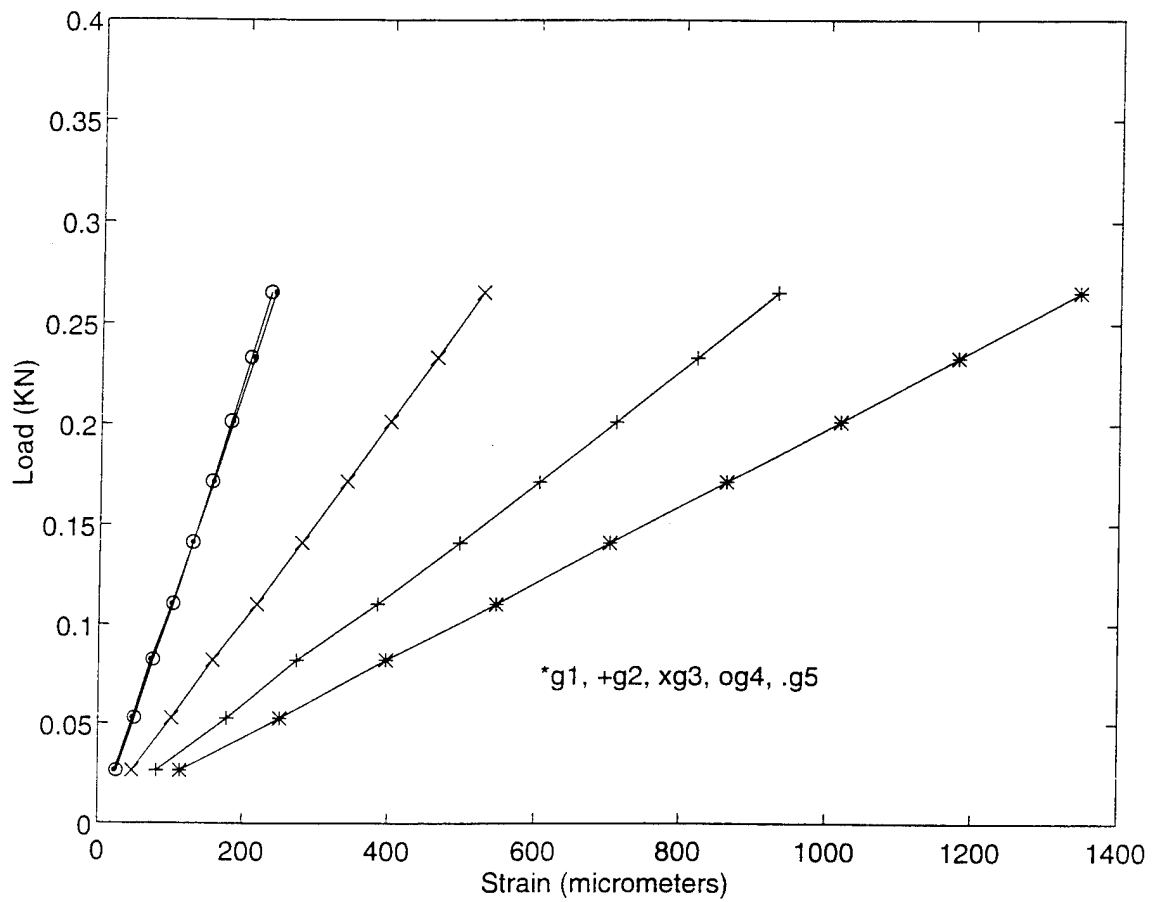


Figure 22. Three Point Bending with 25.40 mm Flat Plates.

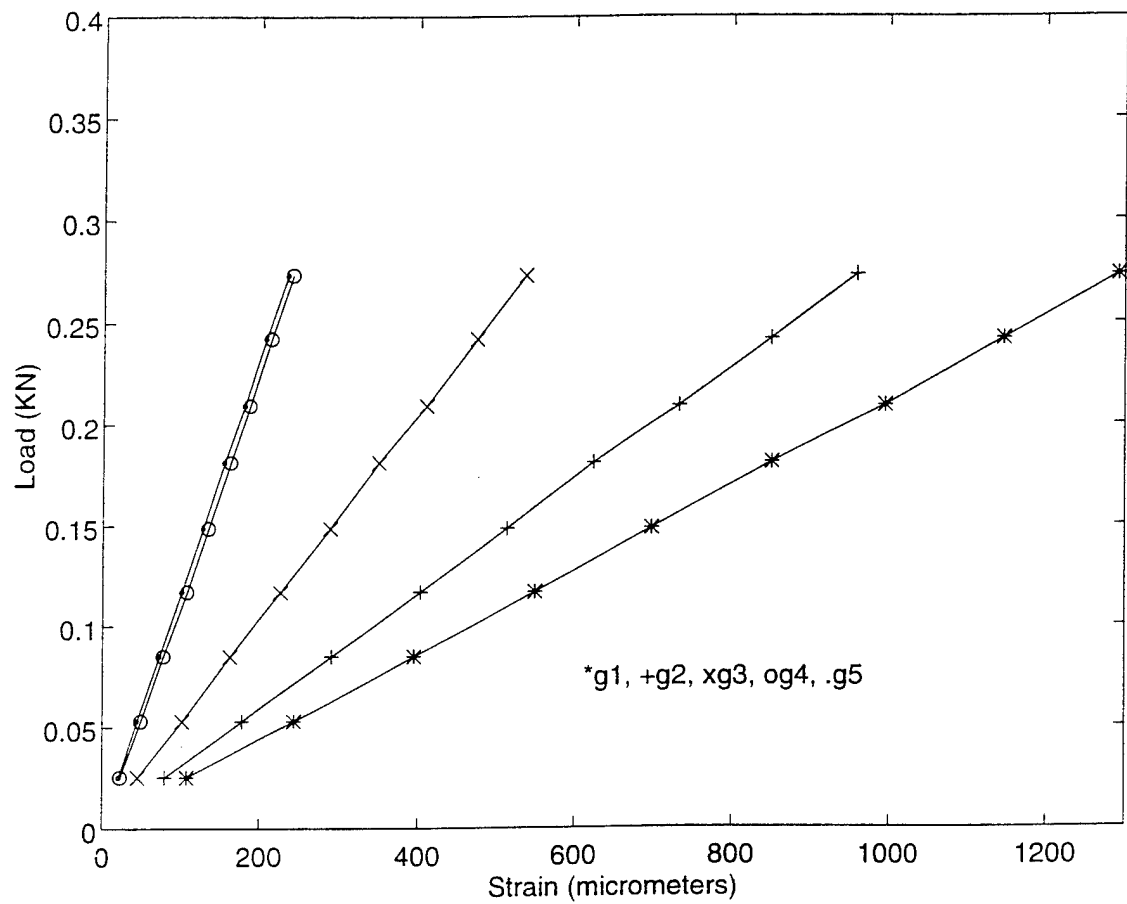


Figure 23. Three Point Bending with 31.75 mm Flat Plates.

load (KN)	gauge1	gauge2	gauge3	gauge4	gauge5
0.03	107	79	45	23	21
0.05	243	178	101	49	44
0.08	395	289	162	77	72
0.12	550	403	226	107	100
0.15	699	514	287	134	127
0.18	850	624	349	162	154
0.21	995	733	410	187	180
0.24	1147	849	474	214	207
0.27	1292	959	537	240	234

Table 13. Results for Three Point Bending with 31.75 mm Flat Plates.

load (KN)	gauge1	gauge2	gauge3	gauge4	gauge5
0.04	73	78	82	33	32
0.08	147	152	164	63	64
0.11	218	224	245	94	95
0.15	289	297	328	125	126
0.18	364	371	414	157	159
0.22	438	448	501	188	191
0.26	521	532	598	222	227
0.29	581	593	669	248	252
0.32	644	656	743	272	280

Table 14. Results for Four Point Bending with 25.4 mm Flat Plates.

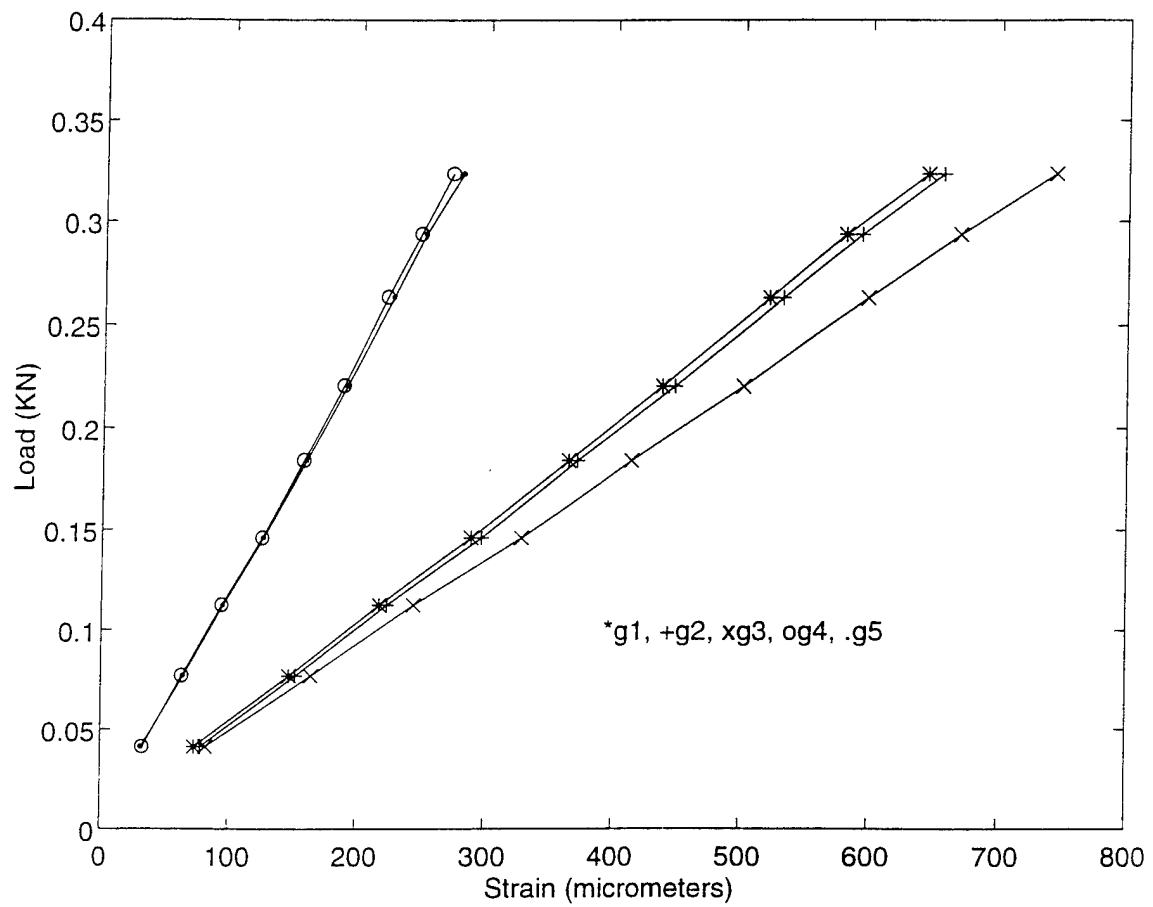


Figure 24. Four Point Bending with 25.4 mm Flat Plates.

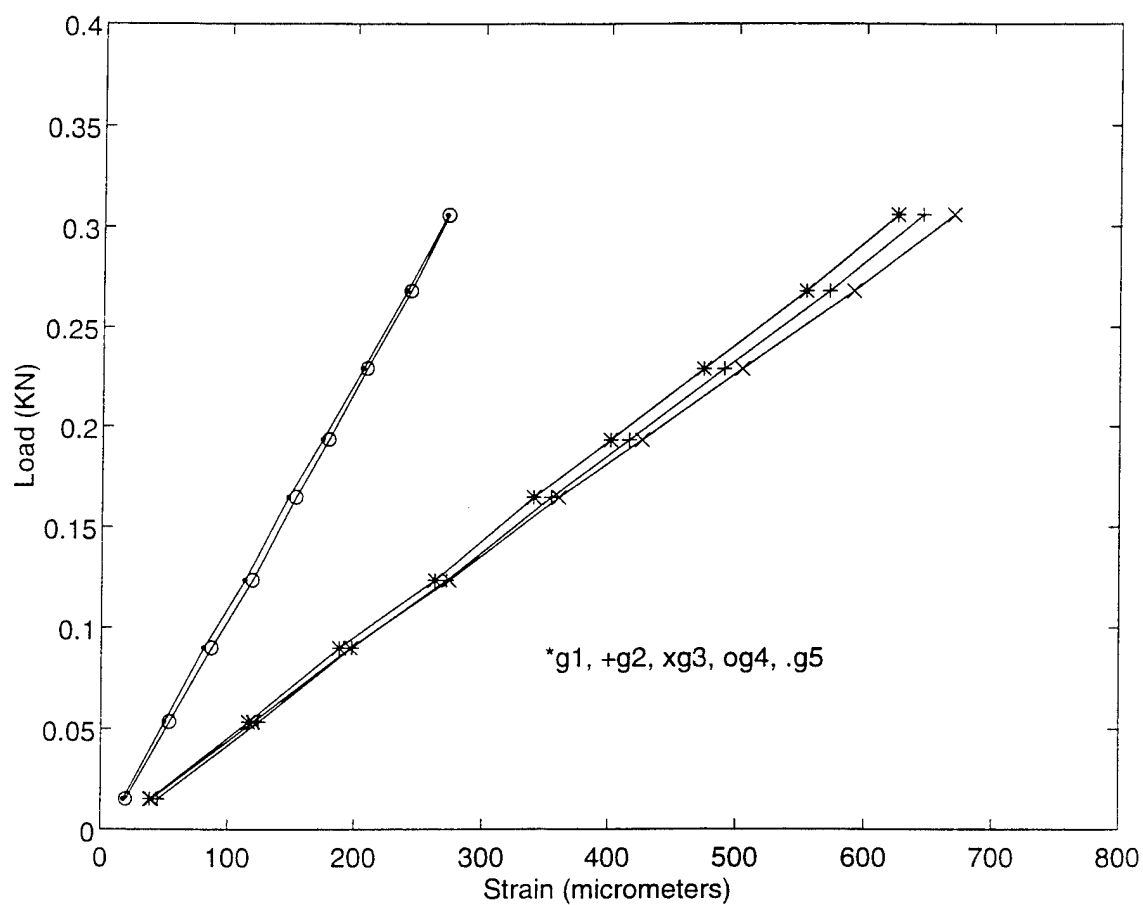


Figure 25. Four Point Bending with 31.75 mm Flat Plates.

load (KN)	gauge1	gauge2	gauge3	gauge4	gauge5
0.02	39	45	40	20	18
0.05	116	124	120	54	50
0.09	188	198	197	87	81
0.12	263	272	274	119	113
0.16	340	354	360	153	147
0.19	401	416	426	179	174
0.23	474	490	504	209	206
0.27	554	572	591	243	240
0.31	625	645	669	272	271

Table 15. Results for Four Point Bending with 31.75 mm Flat Plates.

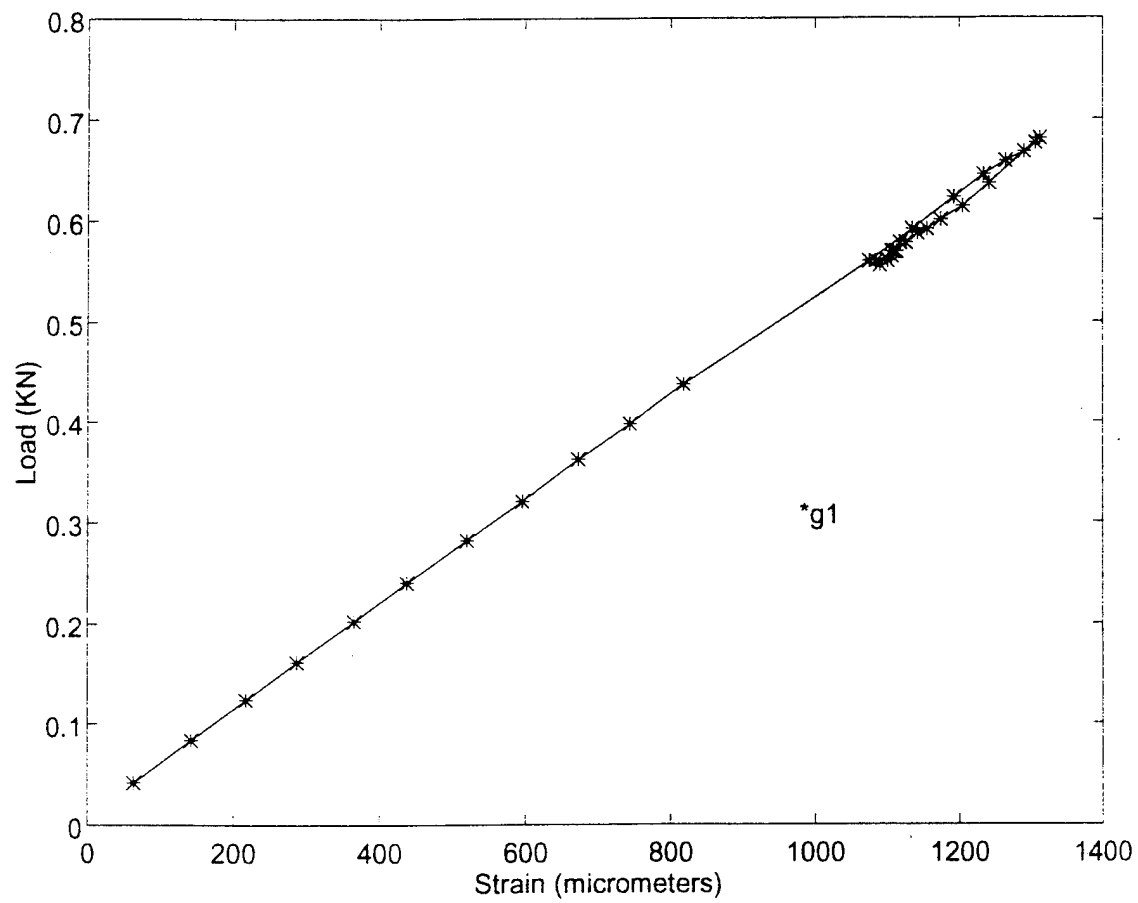


Figure 26. Four Point Bending to Failure with 31.75 mm Flat Plates.

load (KN)	gauge1
0.04	64
0.08	143
0.12	217
0.16	287
0.20	365
0.24	437
0.28	520
0.32	596
0.36	672
0.40	743
0.44	818
0.56	1075
0.59	1134
0.62	1192
0.64	1233
0.66	1264
0.67	1290
0.68	1306
0.68	1312
0.67	1290
0.64	1241
0.61	1204
0.60	1174
0.59	1155
0.59	1142
0.58	1125
0.57	1112

Table 16. Results for Four Point Bending to Failure with 31.75 mm Flat Plates.

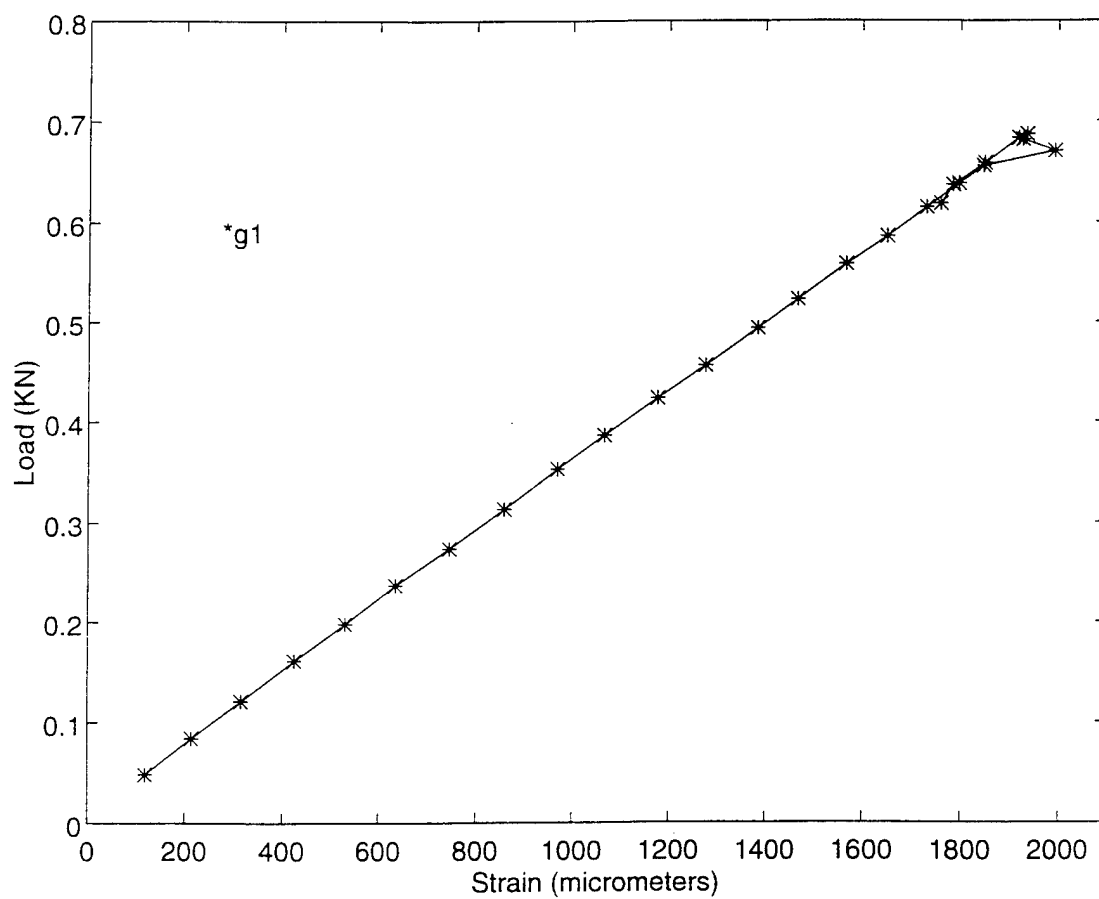


Figure 27. Four Point Bending to Failure with One 12.70 mm Dia. Hole and 31.75 mm Flat Plates.

load (KN)	gauge1
0.05	119
0.08	214
0.12	316
0.16	425
0.20	530
0.24	636
0.27	746
0.31	859
0.35	970
0.39	1067
0.42	1178
0.46	1276
0.49	1385
0.52	1469
0.56	1568
0.59	1651
0.62	1731
0.64	1797
0.66	1848
0.67	1993
0.68	1927
0.69	1936
0.68	1919
0.66	1850
0.64	1785
0.62	1760

Table 17. Results for Four Point Bending to Failure with One 12.70 mm Dia. Hole and 31.75 mm Flat Plates.

V. COMPRESSION TEST

Having determined that the bending test was ineffective in evaluating the effect of stress concentration around a hole in foam cored composite beams, compression testing was pursued using pinned-pinned end conditions as described in Chapter III. The results of the compression testing are not discussed in a chronological order as was the case in chapter IV. First, the tests conducted are listed along with the associated tables and figures. This is followed by a summary of results in table format. A discussion of trends concludes this chapter.

Two tests were conducted on samples with 3 mm (0.12 in.) thick foam. The first sample had a 12.70 mm (0.5 in.) hole at the center. The second sample had a 22.23 mm (0.875 in.) hole at the center. Figures 28 and 29 and Tables 18 and 19 show the results. Strain gauges were located in accordance with Figure 30 for all three tests.

Four tests were conducted on the samples with 6.35 mm (0.25 in.) thick foam. The first two samples had a 12.70 mm (0.5 in.) hole at the center and a 19.05 mm (0.75 in.) hole at the center respectively with strain gauges mounted as shown in Figure 30. See Figures 31 and 32 and Tables 20 and 21 for the test data. The third and fourth samples respectively had 12.70 mm (0.5 in.) and 19.05 mm (0.75 in.) holes at the quarter points. See Figures 33 and 34 and Tables 22 and 23 for the results. The strain gauges were located as shown in Figure 35.

Six tests were conducted on samples with 12.70 mm (0.5 in.) thick foam. The first three samples had a 6.35 mm (0.25 in.) hole at the center, a 12.70 mm (0.5 in.) hole at the center, and a 19.05 mm (0.75 in.) hole at the center respectively. See Figures 36, 37, and 38 and Tables 24, 25, and 26 for the results. Strain gauge locations are shown in Figure 30. The fourth sample had a 6.35 mm (0.25 in.) hole at one quarter point with strain gauge locations as in Figure 39. See Figure 40 and Table 27. The fifth sample had a 6.35 mm (0.25 in.) hole at both quarter points with strain gauge locations as shown in Figure 35. See Figure 41 and Table 28. The sixth sample had a 6.35 mm (0.25 in.) hole at each quarter point and at the center, with strain gauge locations as shown in Figure 42. The results are shown in Figure 43 and Table 29.

Referring to Table 30, the compression test results will now be discussed. Prior to failure, each compressed sample took a characteristic shape as shown in Figure 44. The strain diagrams indicate a trend described by initial column compression followed by column bending.

The sample with a core thickness of 3 mm (0.12 in.) without a circular hole failed at a load of 3.47 KN at the quarter point, [Ref. 2]. The same size sample when subjected to a 12.70 mm (0.5 in.) circular hole at the center failed at 2.74 KN at the quarter point for a load reduction of 21 percent. When subjected to a 22.23 mm (0.875 in.) hole, the sample failed at 2.61 KN at the center for a reduction of 24.8 percent. When failure occurred at the quarter point away from the hole, foam core shear failure and delamination were evident. The carbon skin was left intact. When failure occurred at the hole, failure by bending was evident as the

carbon skin also failed.

The sample with a 6.35 mm (0.25 in.) thick core without a hole failed at 6.31 KN at the quarter point, [Ref. 2]. With a 12.70 mm (0.5 in.) centered hole, it failed at 6.13 KN at the quarter point for a 3.0 percent reduction. When the hole was increased to 19.05 mm (0.75 in.) the sample failed at 5.24 KN at the center for a reduction of 17.1 percent. The tests conducted on the samples with a core thickness of 6.35 mm (0.25 in.) followed the same trend as the tests conducted on the sample with a core thickness of 3 mm (0.12 in.). Failure by bending occurred when the hole diameter was 19.05 mm (0.75 in.), vice 22.23 mm (.875 in.) for the sample with the 3 mm (0.12 in.) thick core.

The sample with a 12.70 mm (0.5 in.) thick core without a hole failed at 14.23 KN at the quarter point, [Ref. 2]. A 6.35 mm (0.25 in.) hole reduced the failure load by 13.5 percent. The transition to failing at the center occurred when subjected to a 12.70 mm (0.5 in.) hole at the center. This resulted in a failure load reduction of 28.1 percent. The tests show that a foam cored sandwich composite beam subjected to stress concentration at a hole and loaded in compression with pinned-pinned end conditions fails at a reduced load. The beam fails at the quarter point by foam core shear failure until the hole reaches a critical diameter at which point the beam fails by bending failure at the hole. The critical diameter decreases as the foam core thickness increases.

Further tests were conducted locating the circular hole at the quarter point of the beam. Using a sample with a core thickness of 6.35 mm (0.25 in.), a test was conducted with a 12.70 mm (0.5 in.) hole at each quarter point. The beam failed at 5.74 KN at the quarter

point for a reduction in failure load of 9.2 percent when compared to the no-hole sample. When this sample was subjected to a 19.05 mm (0.75 in.) hole at each quarter point, the failure occurred at 4.99 KN at the quarter point for a reduction of 21.0 percent. In general, the failure load decreased when the location of a given diameter hole was moved from the center to the quarter point, with failure occurring at the quarter point.

Similar tests were conducted on the samples with a foam thickness of 12.70 mm (0.5 in.). A sample with a 6.35 mm (0.25 in.) hole at one quarter point failed at 13.41 KN at the quarter point. A sample with a 6.35 mm (0.25 in.) hole at each quarter point failed at 13.21 KN at the quarter point. A sample with 6.35 mm (0.25 in.) holes at the center and at both quarter points failed at 13.15 KN at the quarter point. These failure loads are approximately 7 percent lower than the no-hole failure load. Unlike the samples with 6.35 mm (0.25 in.) thick cores, the samples with 12.70 mm (0.5 in.) thick cores failed at slightly higher loads when the hole was moved from the center to the quarter point. The experimental failure load for the sample with a 6.35 mm (0.25 in.) hole at the center is inconsistent compared to other test results. This may be due to a variation in specimen geometry or an experimental error. It is recommended that this test be repeated for accuracy.

Having established the trends within each sample thickness category, the discussion will now turn to an analysis across sample thickness groups, holding circular hole locations constant.

The 6.35 mm (0.25 in.) thick foam is 112 percent thicker than the 3 mm (0.12 in.) foam while the 12.70 mm (0.5 in.) foam is 100 percent thicker than the 6.35 mm (0.25 in.)

foam. With no hole, the failure load increases by 82 percent when increasing foam thickness from 3mm (0.12 in.) to 6.35mm (0.25 in.) and by 125 percent when increasing from 6.35 mm (0.25 in.) to 12.70 mm (0.5 in.).

When subjected to a 12.70 mm (0.5 in.) hole at the center, the failure load increased by 124 percent when increasing foam thickness from 3 mm (0.12 in.) to 6.35 mm (0.5 in.). A comparison cannot be made to the sample with 12.70 mm (0.5 in.) thick foam as the sample failed at the center vice the quarter point.

When subjected to a 19.05 mm (0.75 in.) hole at the center, the failure load increased by 96 percent when increasing from a foam thickness of 6.35 mm (0.25 in.) to 12.70 mm (0.5 in.).

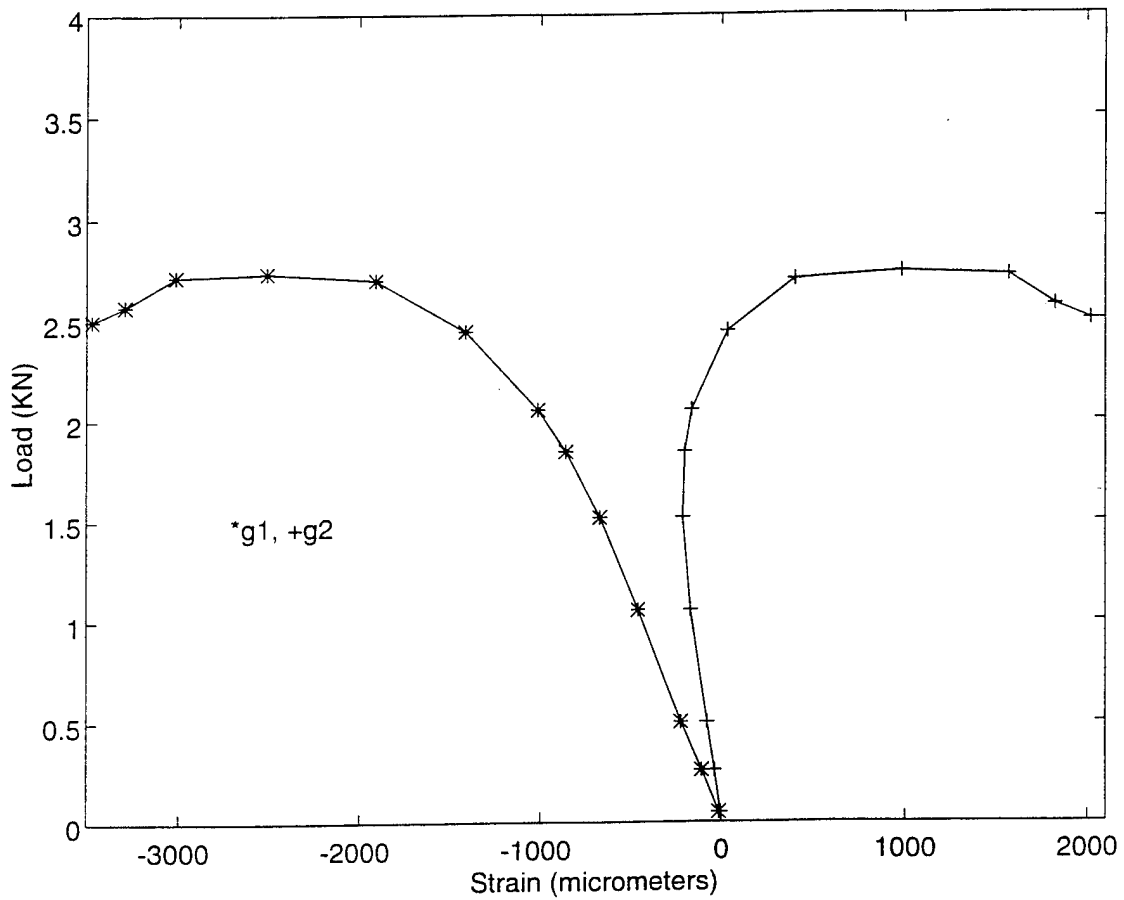


Figure 28. Compression Test, 3 mm Thick, One 12.70 mm Dia. Hole at the Center.

load (KN)	gauge1	gauge2
0.05	-14	-5
0.26	-106	-36
0.50	-219	-78
1.05	-460	-168
1.52	-675	-210
1.85	-861	-200
2.06	-1013	-162
2.45	-1412	33
2.70	-1909	402
2.74	-2511	984
2.72	-3016	1565
2.57	-3290	1823
2.50	-3470	2020

Table 18. Compression Test, 3 mm Thick, One 12.70 mm Dia. Hole at the Center.

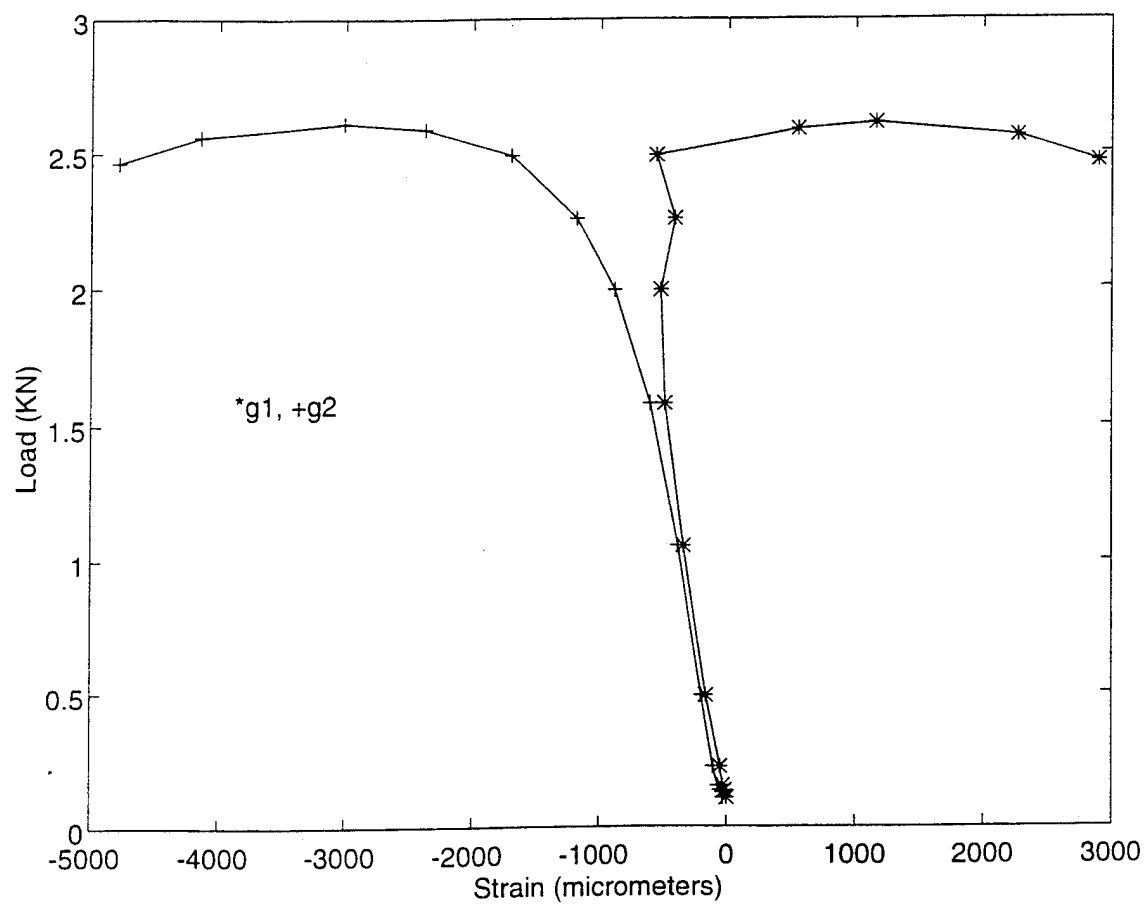


Figure 29. Compression Test, 3 mm Thick, One 22.23 mm Dia. Hole at the Center.

load (KN)	gauge1	gauge2
0.11	0	-30
0.13	-15	-52
0.15	-30	-70
0.22	-50	-105
0.49	-163	-199
1.05	-340	-382
1.58	-484	-597
1.99	-520	-880
2.26	-414	-1188
2.49	-56	-1704
2.59	545	-2382
2.61	1155	-3014
2.56	2268	-4146
2.46	2896	-4786

Table 19. Compression Test, 3 mm Thick, One 22.23 mm Dia. Hole at the Center..

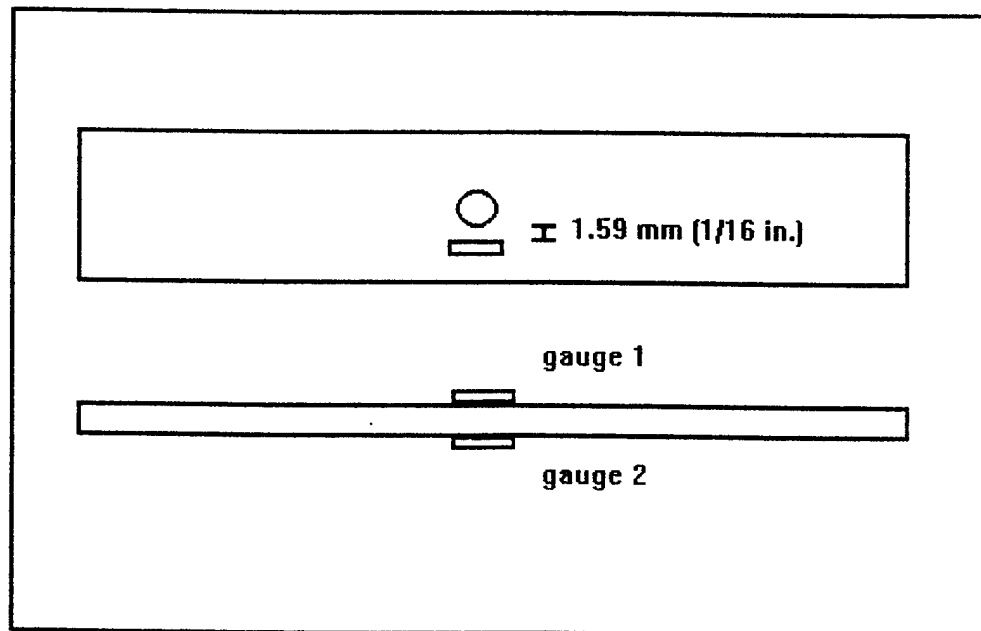


Figure 30. Strain Gauge Locations for 3 mm Thick Compression Tests.

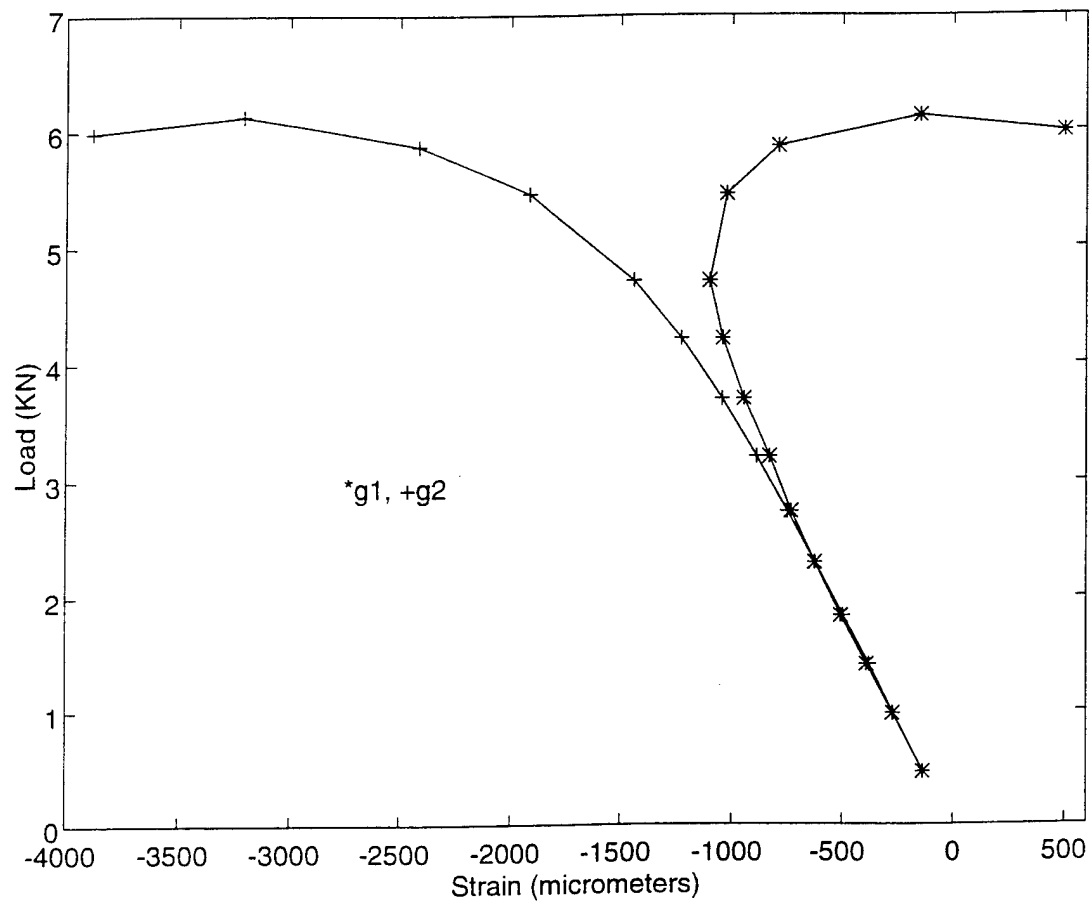


Figure 31. Compression Test, 6.35 mm Thick, One 12.70 mm Dia. Hole at the Center.

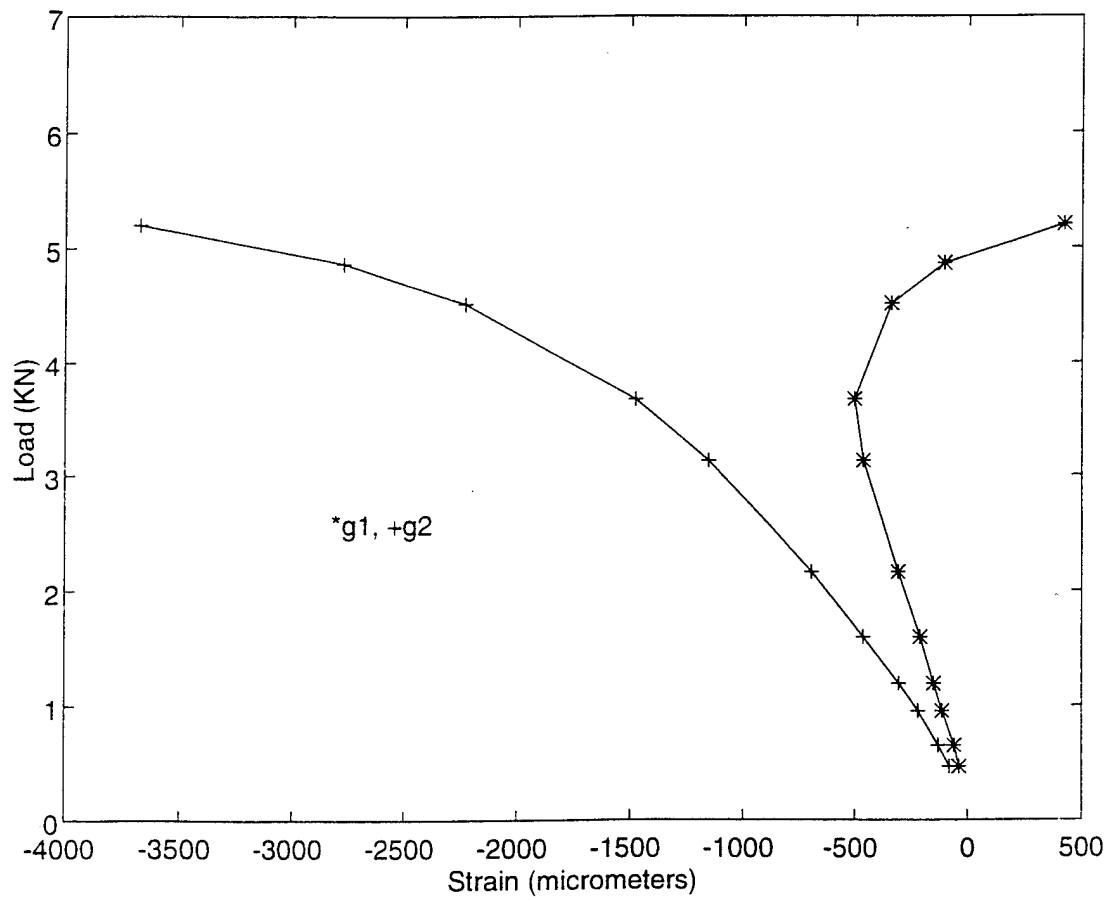


Figure 32. Compression Test, 6.35 mm Thick, One 19.05 mm Dia. Hole at the Center.

load (KN)	gauge1	gauge2
0.46	-135	-135
0.98	-272	-270
1.41	-391	-380
1.84	-506	-497
2.30	-624	-622
2.74	-732	-749
3.21	-830	-890
3.70	-947	-1045
4.22	-1043	-1228
4.72	-1102	-1440
5.46	-1026	-1914
5.87	-792	-2417
6.13	-150	-3209
5.99	500	-3884

Table 20. Compression Test, 6.35 mm Thick, One 12.70 mm Dia. Hole at the Center.

load (KN)	gauge1	gauge2
0.47	-37	-80
0.65	-59	-130
0.96	-112	-218
1.19	-150	-303
1.60	-210	-463
2.16	-307	-694
3.13	-463	-1153
3.68	-503	-1477
4.52	-339	-2229
4.87	-105	-2775
5.20	420	-3672
5.24		-4689

Table 21. Compression Test, 6.35 mm Thick, One 19.05 mm Dia. Hole at the Center.

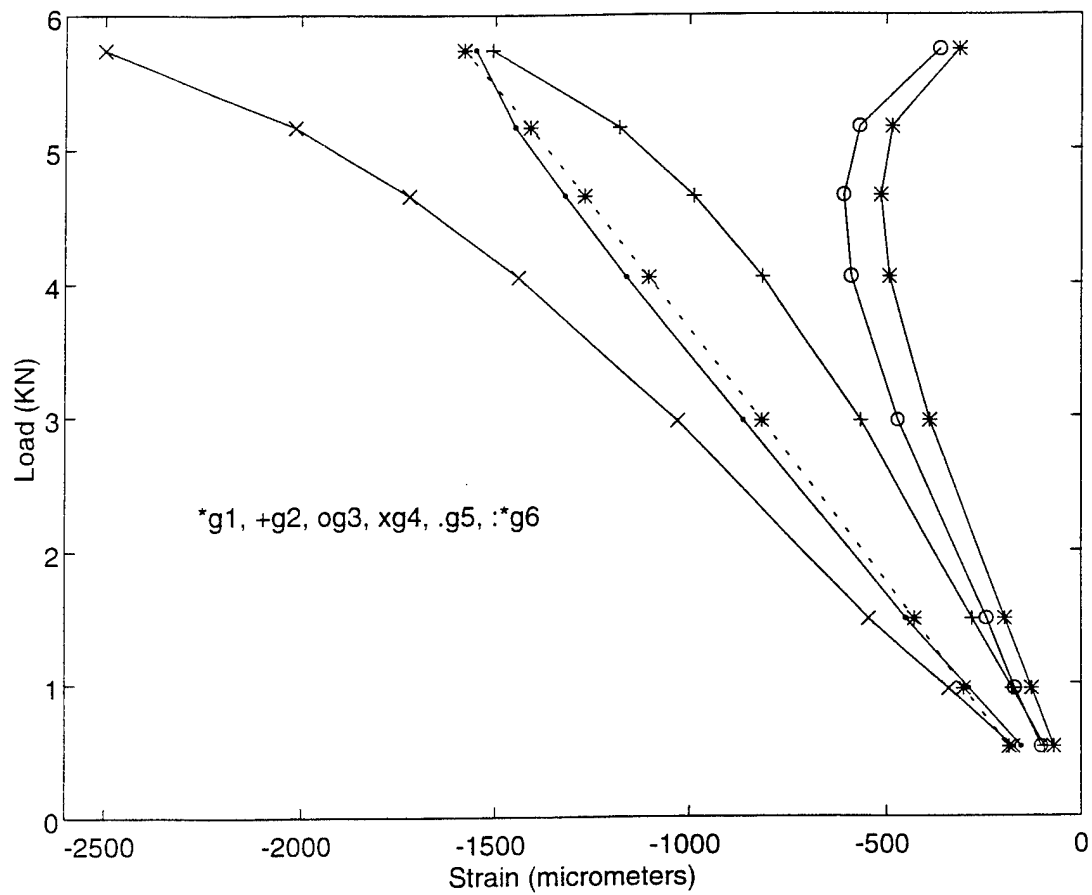


Figure 33. Compression Test, 6.35 mm Thick, One 12.70 mm Dia. Hole at Each Quarter Point.

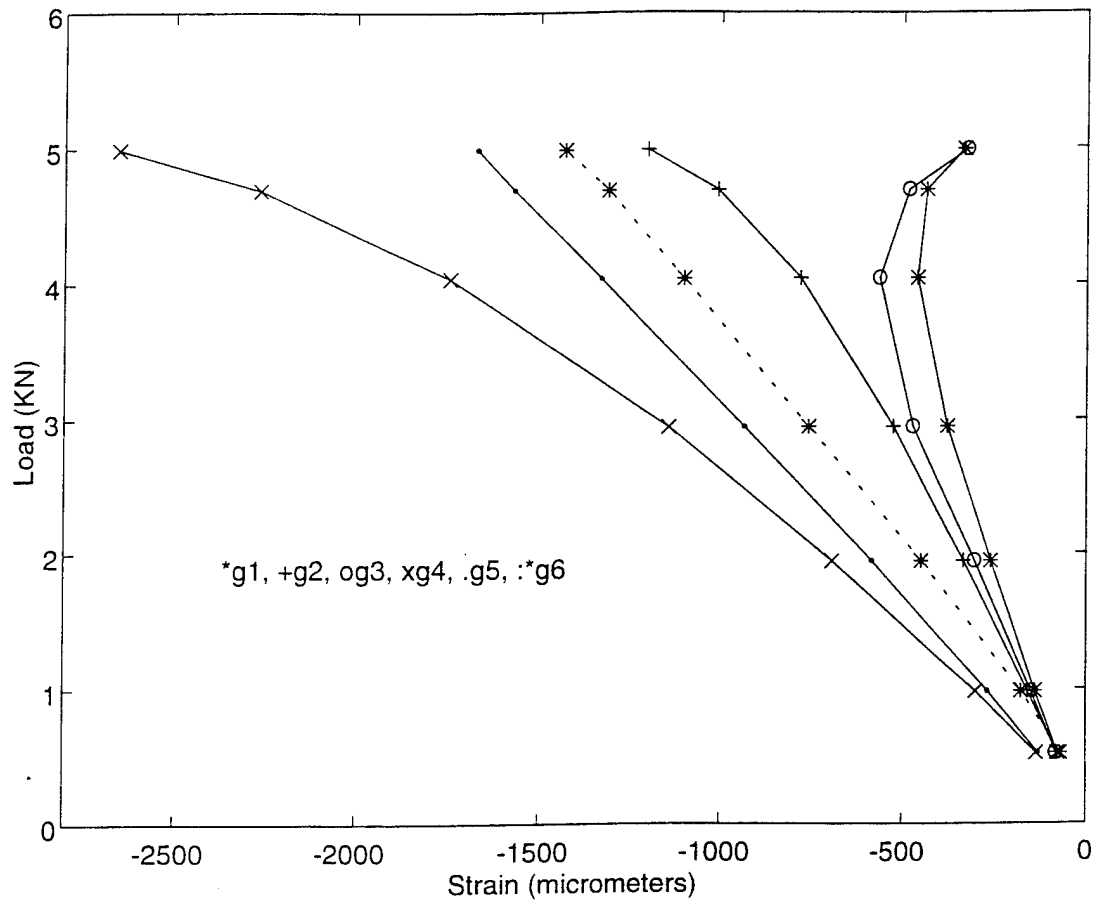


Figure 34. Compression Test, 6.35 mm Thick, One 19.05 mm Dia. Hole at Each Quarter Point.

load (KN)	gauge1	gauge2	gauge3	gauge4	gauge5	gauge6
0.52	-70	-95	-103	-175	-154	-185
0.96	-127	-177	-171	-340	-288	-302
1.49	-196	-280	-243	-546	-449	-427
2.97	-388	-566	-470	-1030	-863	-815
4.05	-492	-814	-590	-1439	-1159	-1103
4.65	-514	-989	-609	-1720	-1320	-1269
5.16	-485	-1179	-569	-2015	-1448	-1410
5.74	-313	-1507	-362	-2500	-1549	-1579

Table 22. Compression Test, 6.35 mm Thick, One 12.70 mm Dia. Hole at Each Quarter Point.

load (KN)	gauge1	gauge2	gauge3	gauge4	gauge5	gauge6
0.52	-76	-78	-80	-133	-128	-68
0.98	-137	-157	-148	-299	-266	-175
1.94	-258	-333	-303	-694	-585	-448
2.95	-377	-526	-471	-1140	-933	-758
4.04	-460	-782	-565	-1744	-1328	-1100
4.69	-435	-1008	-483	-2266	-1569	-1309
4.99	-333	-1199	-324	-2652	-1670	-1430

Table 23. Compression Test, 6.35 mm Thick, One 19.05 mm Dia. Hole at Each Quarter Point.

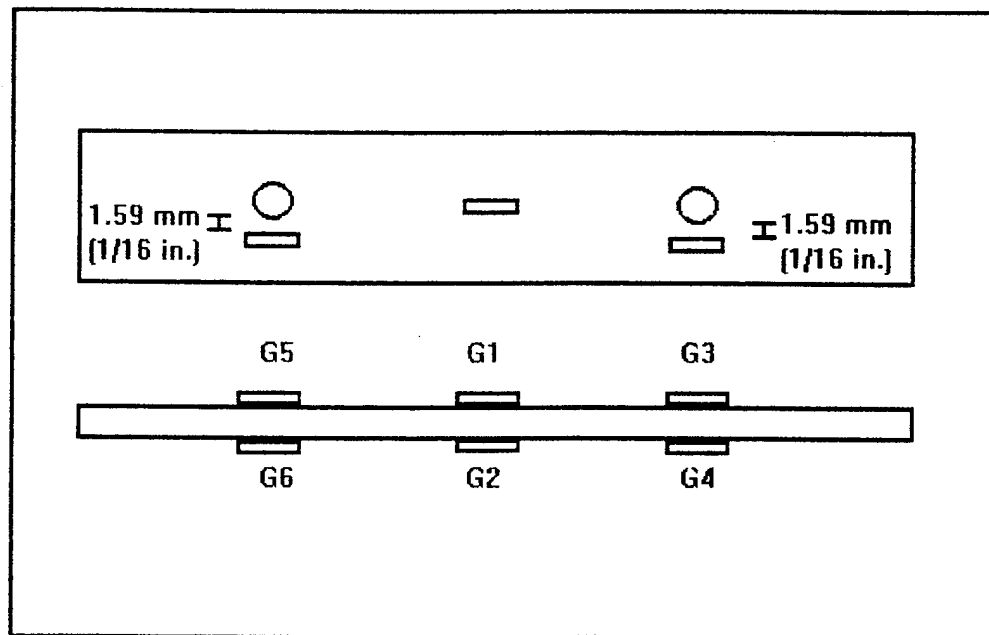


Figure 35. Strain Gauge Locations for Samples with Holes at Quarter Points.

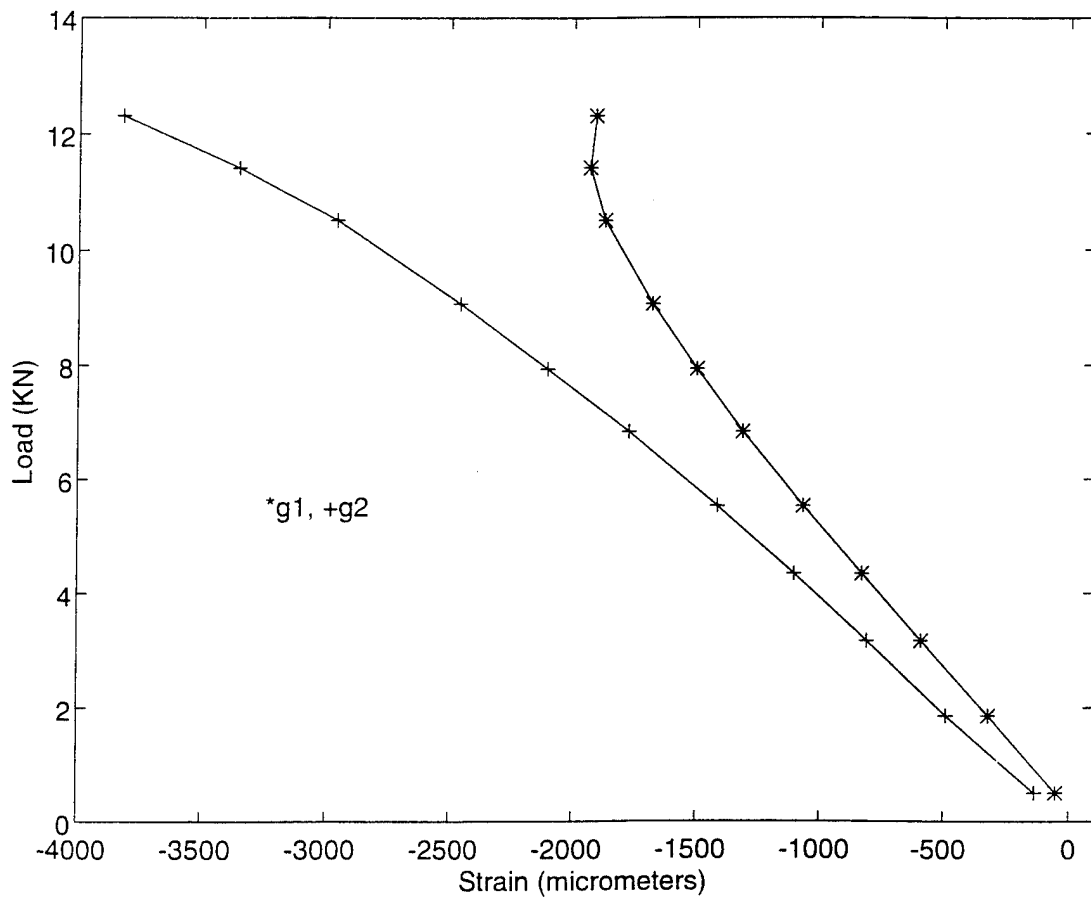


Figure 36. Compression Test, 12.70 mm Thick, 6.35 mm Dia. Hole at the Center.

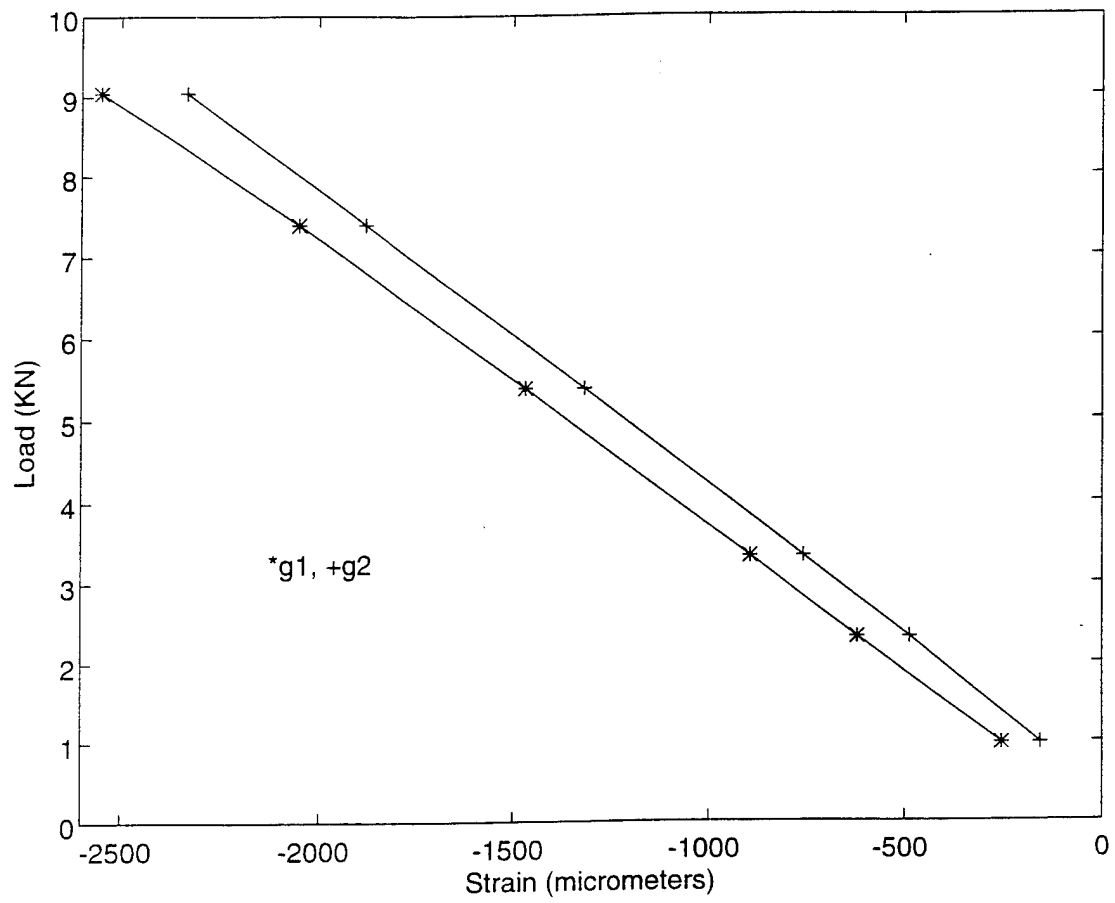


Figure 37. Compression Test, 12.70 mm Thick, 12.70 mm Dia. Hole at the Center.

load (KN)	gauge1	gauge2
0.50	-52	-135
1.86	-319	-489
3.17	-590	-809
4.35	-829	-1102
5.54	-1066	-1413
6.84	-1311	-1770
7.94	-1497	-2100
9.07	-1677	-2456
10.52	-1822	-2958
11.42	-1934	-3353
12.31	-1911	-3820

Table 24. Compression Test, 12.70 mm Thick, 6.35 mm Dia. Hole at the Center.

load (KN)	gauge1	gauge2
0.98	-254	-157
2.33	-620	-487
3.34	-895	-757
5.39	-1468	-1317
7.40	-2049	-1878
9.04	-2550	-2335
10.23		

Table 25. Compression Test, 12.70 mm Thick, 12.70 mm Dia. Hole at the Center.

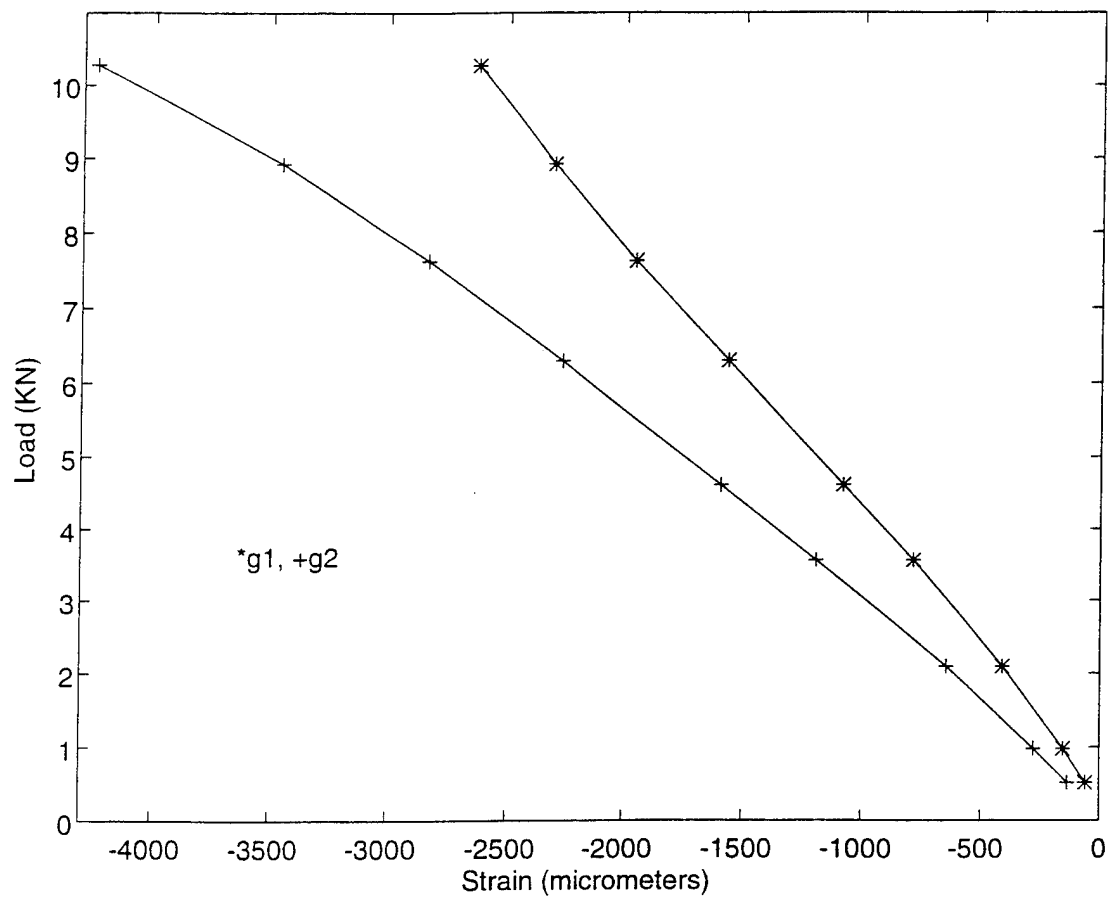


Figure 38. Compression Test, 12.70 mm Thick, 19.05 mm Dia. Hole at the Center.

load (KN)	gauge1	gauge2
0.51	-58	-134
0.98	-152	-277
2.10	-410	-647
3.56	-786	-1190
4.62	-1078	-1593
6.31	-1564	-2264
7.63	-1953	-2834
8.93	-2303	-3455
10.28	-2629	-4244

Table 26. Compression Test, 12.70 mm Thick, 19.05 mm Dia. Hole at the Center.

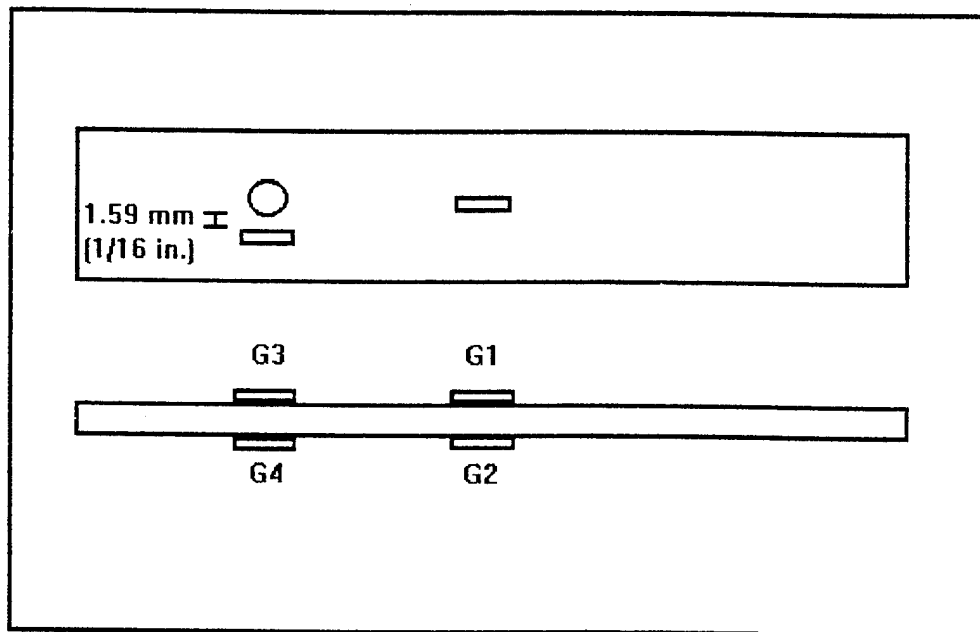


Figure 39. Strain Gauge Location for Samples with One Hole at One Quarter Point.

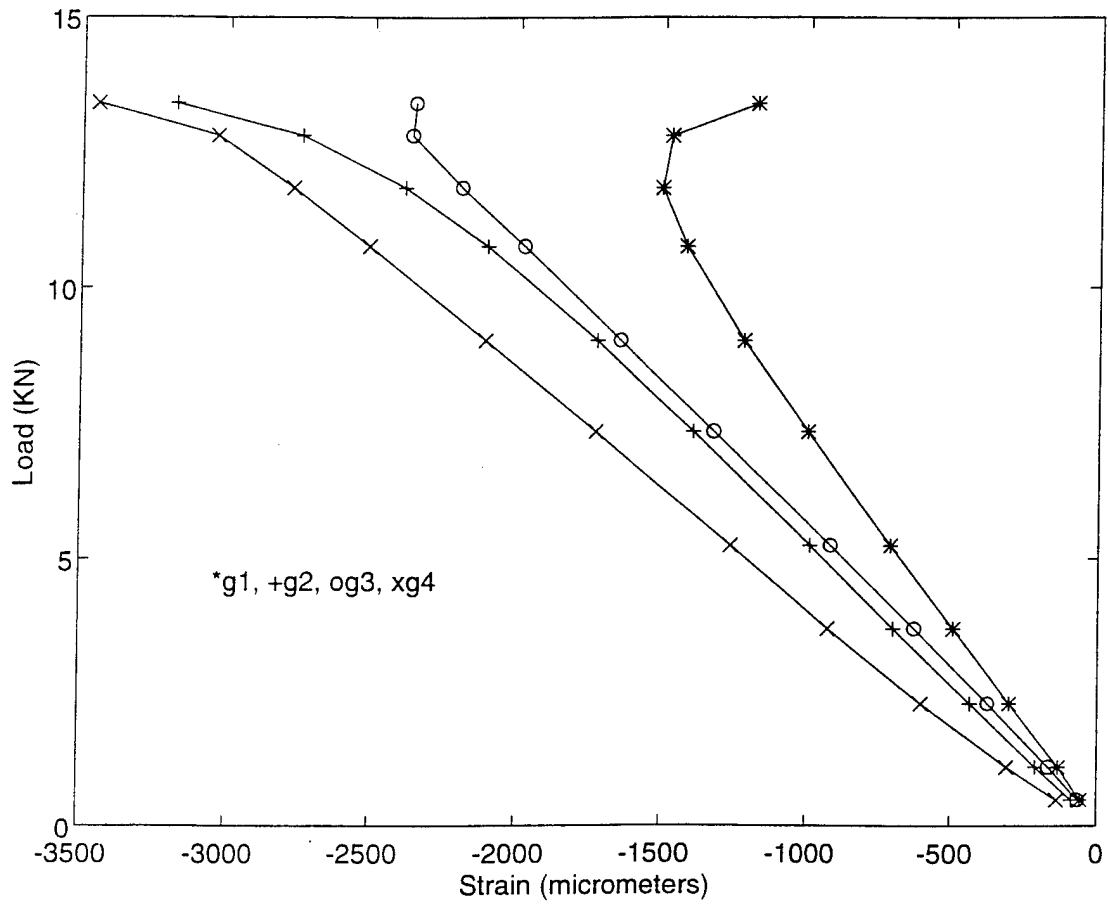


Figure 40. Compression Test, 12.70 mm Thick, One 6.35 mm Dia. Hole at One Quarter Point.

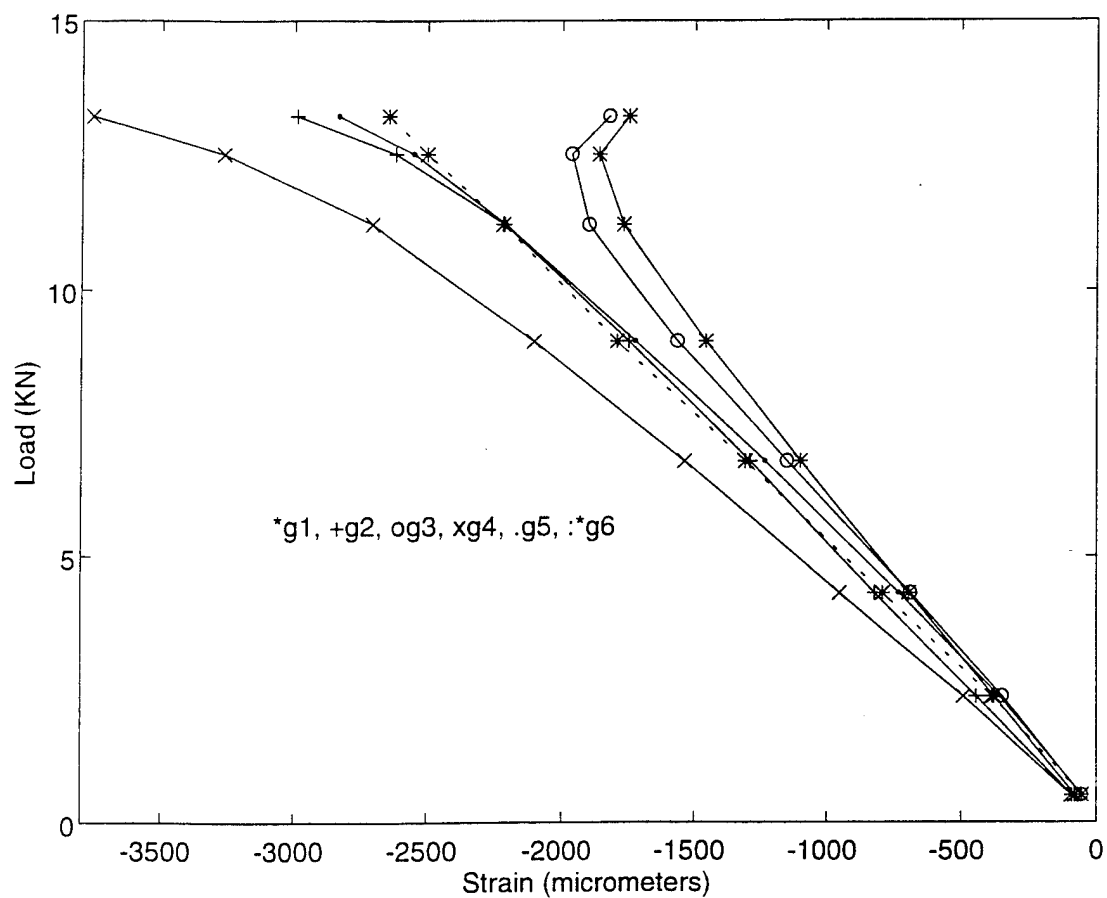


Figure 41. Compression Test, 12.70 mm Thick, 6.35 mm Dia. Hole at Each Quarter Point.

load (KN)	gauge1	gauge2	gauge3	gauge4
0.49	-57	-86	-64	-136
1.11	-132	-208	-164	-307
2.30	-299	-434	-373	-600
3.71	-492	-697	-624	-925
0.52	-707	-988	-916	-1263
7.35	-997	-1393	-1323	-1729
9.03	-1222	-1726	-1645	-2109
10.76	-1420	-2104	-1979	-2510
11.84	-1505	-2390	-2195	-2774
12.81	-1474	-2744	-2368	-3040
13.41	-1183	-3183	-2358	-3450

Table 27. Compression Test, 12.70 mm Thick, One 6.35 mm Dia. Hole at One Quarter Point.

load (KN)	gauge1	gauge2	gauge3	gauge4	gauge5	gauge6
0.50	-80	-92	-57	-94	-53	-54
2.36	-378	-444	-347	-491	-358	-386
4.31	-693	-819	-687	-951	-728	-790
6.77	-1100	-1292	-1152	-1536	-1235	-1310
9.04	-1458	-1744	-1563	-2104	-1718	-1789
11.21	-1765	-2215	-1897	-2705	-2211	-2220
12.51	-1859	-2618	-1964	-3265	-2550	-2500
13.21	-1745	-2990	-1820	-3759	-2833	-2643

Table 28. Compression Test, 12.70 mm Thick, 6.35 mm Dia. Hole at Each Quarter Point.

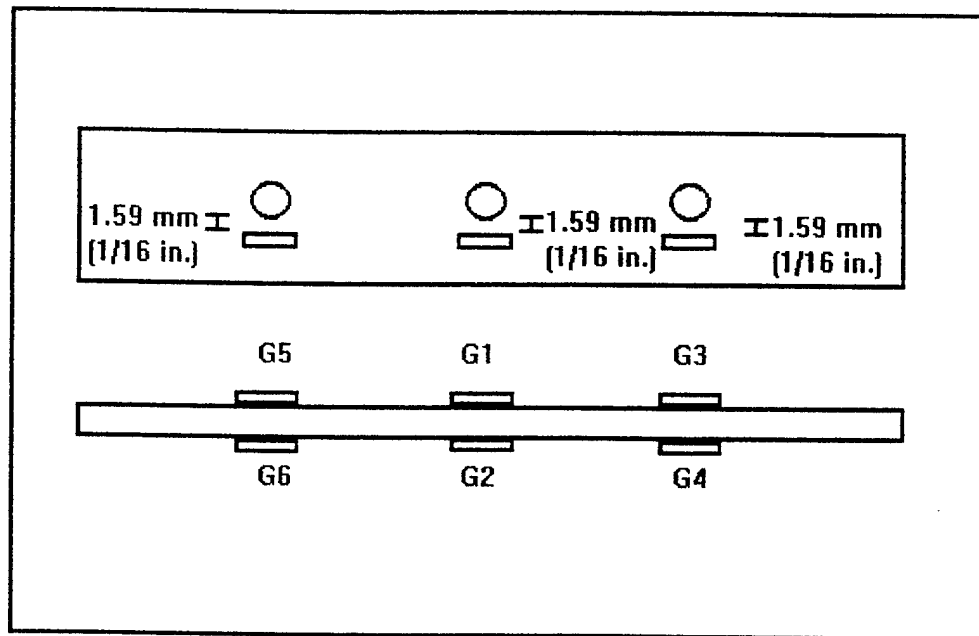


Figure 42. Strain Gauge Locations for Samples with Holes at Each Quarter Point and at the Center.

load (KN)	gauge1	gauge2	gauge3	gauge4	gauge5	gauge6
0.93	-274	-144	-257	-165	-302	-122
2.18	-561	-388	-510	-433	-629	-352
3.81	-898	-728	-809	-811	-1014	-666
6.43	-1453	-1273	-1324	-1402	-1617	-1195
9.15	-2056	-1811	-1872	-2015	-2263	-1722
11.55	-2624	-2285	-2342	-2600	-2896	-2183
12.42	-2821	-2465	-2469	-2854	-3081	-2366
13.15	-2939	-2689	-2510	-3165	-3256	-2521

Table 29. Compression Test, 12.70 mm Thick, 6.35 mm Dia. Hole at Each Quarter Point and at the Center.

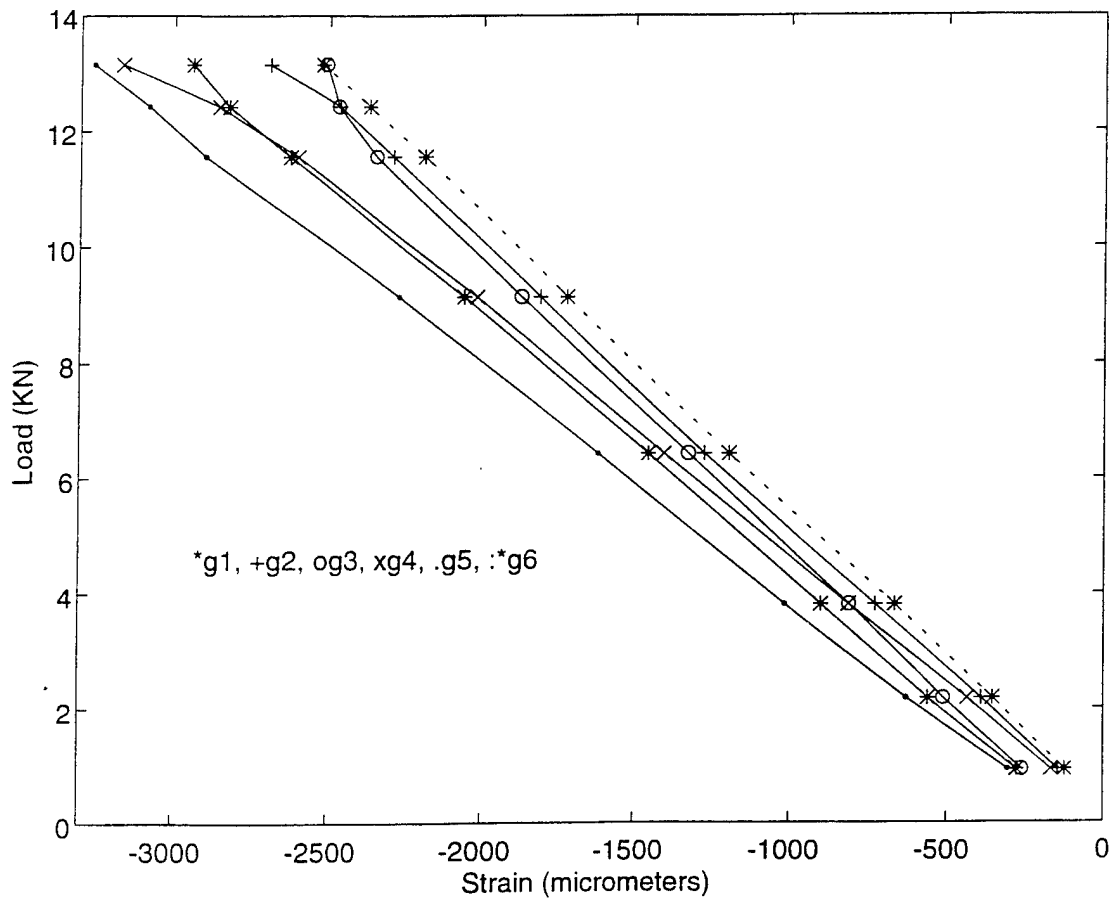


Figure 43. Compression Test, 12.70 mm Thick, 6.35 mm Dia. Hole at Each Quarter Point and at the Center.

	3 mm thick foam	6.35 mm thick foam	12.70 mm thick foam
no hole	3.47 KN at qtr pt	6.32 KN at qtr pt	14.23 KN at qtr pt
6.35mm hole at the center			12.31 KN at qtr pt
12.70 mm hole at the center	2.74 KN at qtr pt	6.13 KN at qtr pt	10.23 KN at center
19.05 mm hole at the center		5.24 KN at center	10.28 KN at center
22.23 mm hole at the center	2.61 KN at center		
6.35 mm hole at one quarter point			13.41 KN at qtr pt
6.35 mm hole at both quarter points			13.21 KN at qtr pt
6.35 mm hole at both quarter points and at center			13.15 KN at qtr pt
12.70 mm hole at both quarter points		5.74 KN at qtr pt	
19.05 mm hole at both quarter points		4.99 KN at qtr pt	

Table 30. Compression Test Summary Chart.

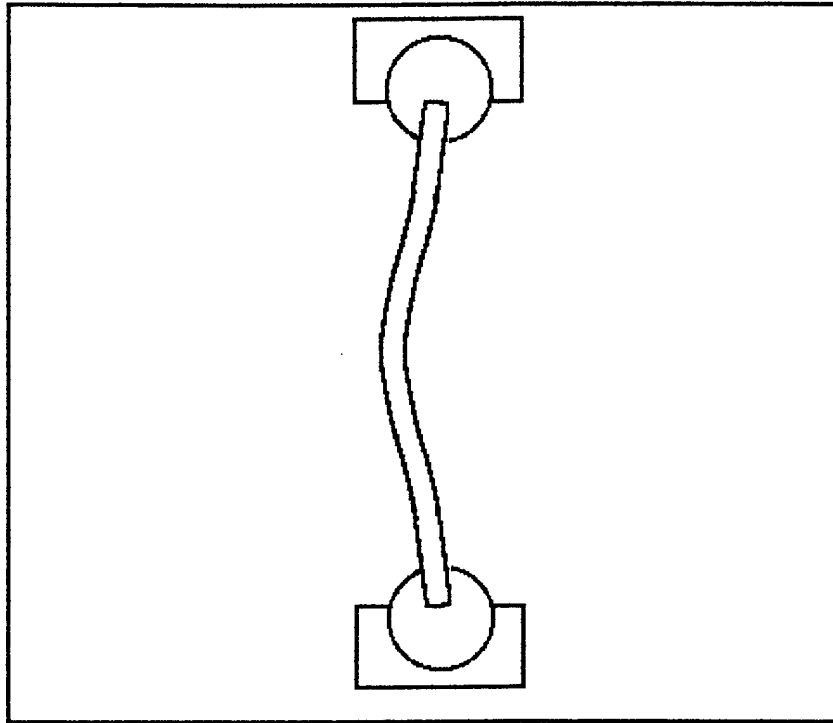


Figure 44. Sample Shape Characteristic of Compression Test.

VI. COMPRESSION WITH DELAMINATION

Four compression tests on delaminated samples were conducted. All four samples had a foam thickness of 6.35 mm (0.25 in.) with a 12.70 mm (0.5 in.) hole at one quarter point. Strain gauges were mounted as shown in Figure 39. Results were compared to the no-hole results obtained from Clawson's study [Ref. 2]. In all cases the delamination was on one side only and was centered length-wise.

The first sample had 101.6 mm (4.0 in.) of delamination and failed by further delamination at a load of 1.1 KN. The failure load was approximately the same as the no-hole failure load obtained by Clawson [Ref. 2]. The results are shown in Figure 45 and Table 31.

The second sample had 50.8 mm (2.0 in.) of delamination and failed by further delamination at a load of 2.7 KN. The failure load was the same as the failure load for the no-hole case. See Figure 46 and Table 32.

The third sample had 25.4 mm (1.0 in.) of delamination and failed at the hole at a load of 4.96 KN. The failure load was 83 percent of the no-hole failure load. Figure 47 and Table 33 shows the results.

The fourth sample had 12.70 mm (0.5 in.) of delamination and failed at the hole at a load of 7.12 KN. The failure load was 93 percent of the no-hole failure load. See Figure 48 and Table 34.

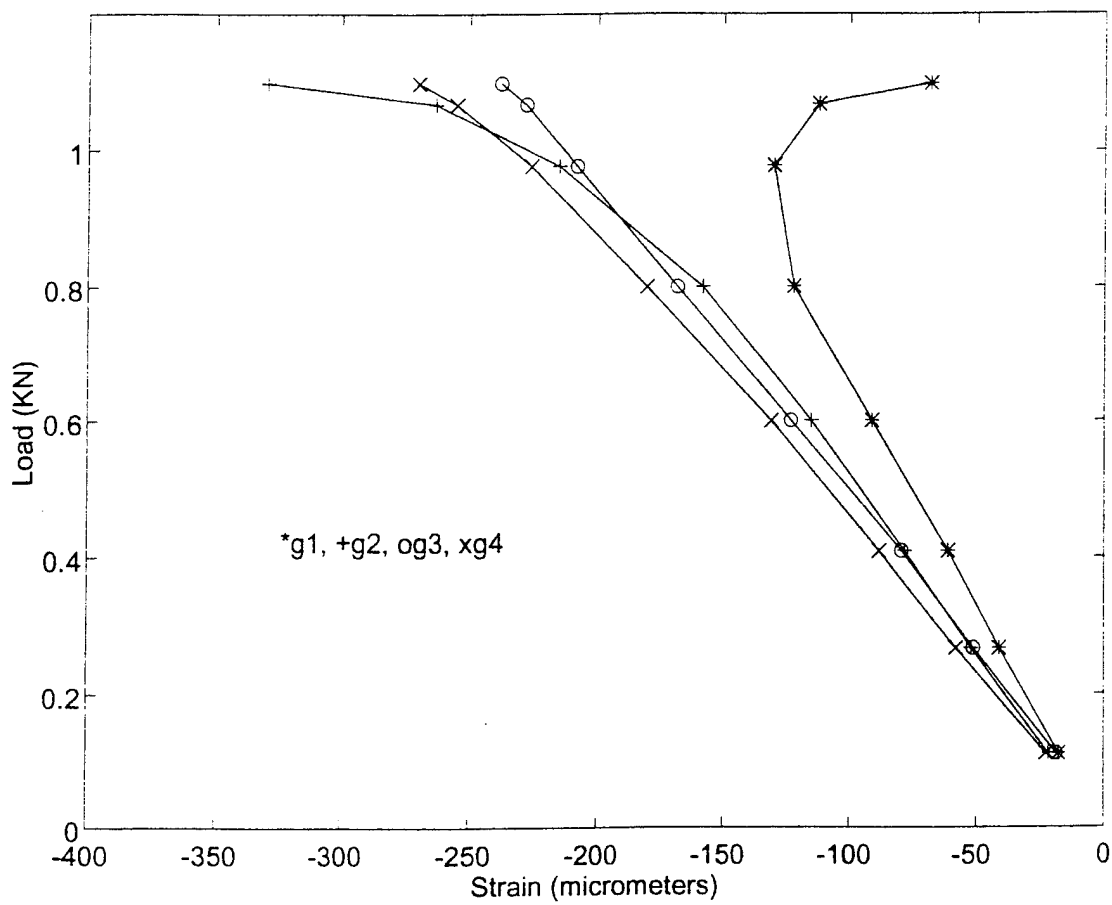


Figure 45. 6.35 mm Thick, 101.6 mm Delamination, 12.70 mm Hole at Quarter Point.

load (KN)	gauge1	gauge2	gauge3	gauge4
0.11	-18	-22	-19	-23
0.27	-41	-52	-51	-58
0.41	-61	-78	-79	-88
0.60	-91	-115	-123	-131
0.80	-122	-158	-168	-180
0.98	-130	-215	-208	-226
1.07	-112	-263	-228	-255
1.10	-68	-330	-238	-270

Table 31. 6.35 mm Thick, 101.6 mm Delamination, 12.70 mm Hole at Quarter Point.

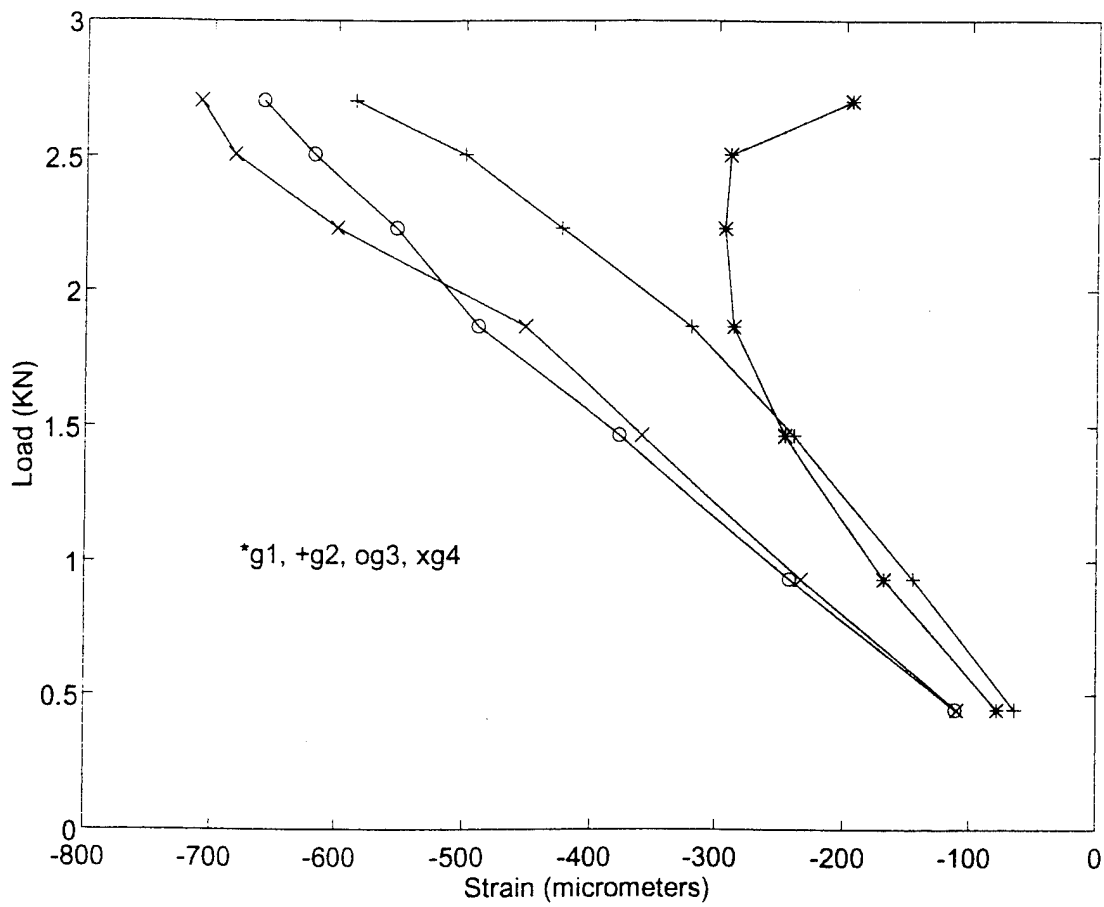


Figure 46. 6.35 mm Thick, 50.8 mm Delamination, 12.70 mm Hole at Quarter Point.

load (KN)	gauge1	gauge2	gauge3	gauge4
0.44	-78	-64	-111	-110
0.93	-168	-145	-242	-233
1.47	-246	-239	-377	-359
1.87	-287	-320	-489	-452
2.24	-294	-424	-553	-600
2.51	-290	-500	-619	-683
2.70	-195	-586	-660	-710

Table 32. 6.35 mm Thick, 50.8 mm Delamination, 12.70 mm Hole at Quarter Point.

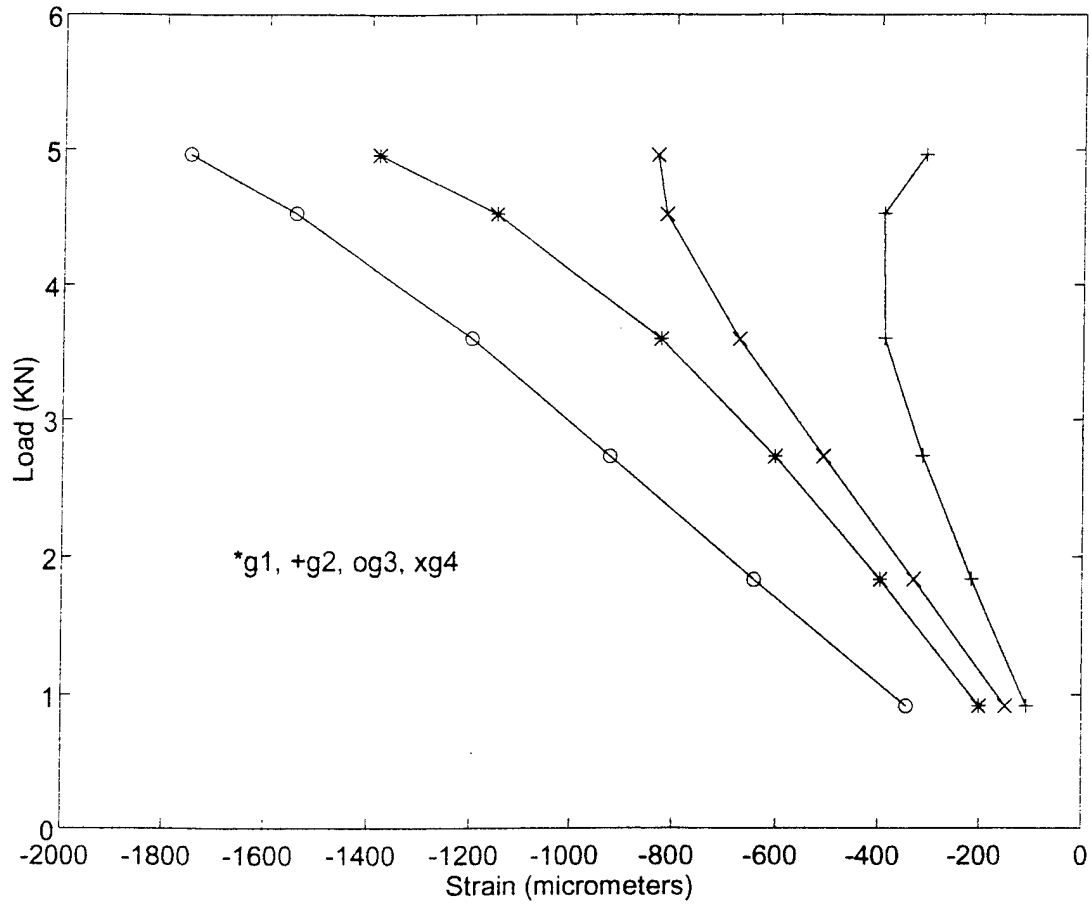


Figure 47. 6.35 mm Thick, 25.4 mm Delamination, 12.70 mm Hole at Quarter Point.

load (kN)	gauge1	gauge2	gauge3	gauge4
0.92	-201	-108	-344	-150
1.84	-397	-217	-644	-331
2.73	-604	-315	-923	-510
3.60	-826	-391	-1200	-676
4.53	-1153	-393	-1545	-817
4.96	-1384	-311	-1752	-835

Table 33. 6.35 mm Thick, 25.4 mm Delamination, 12.70 mm Hole at Quarter Point.

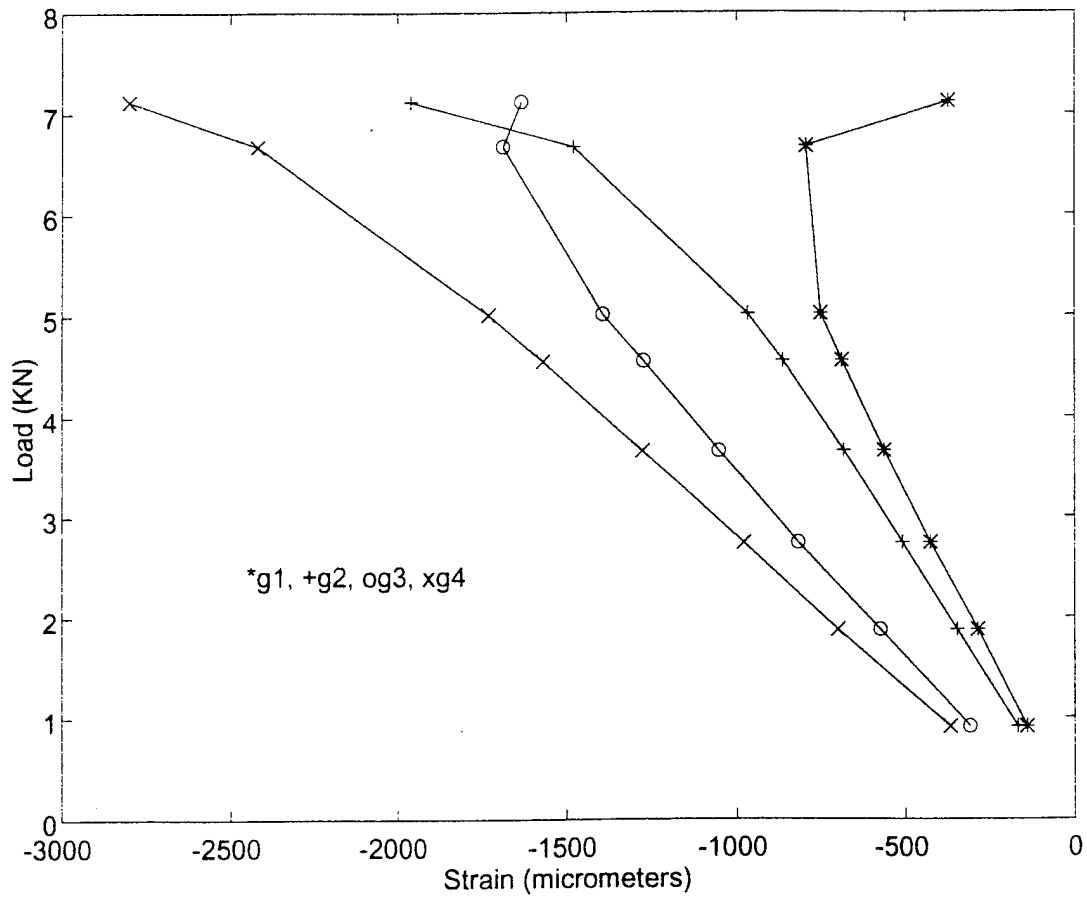


Figure 48. 6.35 mm Thick, 12.70 mm Delamination, 12.70 mm Hole at Quarter Point.

load (KN)	gauge1	gauge2	gauge3	gauge4
0.92	-140	-167	-307	-367
1.88	-284	-347	-572	-700
2.74	-425	-507	-817	-980
3.66	-562	-682	-1051	-1275
4.56	-688	-863	-1271	-1568
5.02	-751	-968	-1390	-1730
6.67	-794	-1477	-1686	-2419
7.12	-372	-1960	-1632	-2800

Table 34. 6.35 mm Thick, 12.70 mm Delamination, 12.70 mm Hole at Quarter Point.

VII. FINITE ELEMENT ANALYSIS

A finite element analysis was conducted to better understand the experimental results. The ANSYS Engineering Analysis System revision 4.4 was used to conduct the numerical modeling. Five models were constructed representing the no-hole case, the center hole case, the quarter point hole case, the case with a hole at each quarter point, and the case with a hole at each quarter point and at the center. Figures 49, 50, 51, 52, and 53 show the element mesh.

A linear buckling analysis was conducted first. Smeared mechanical properties for the composite were calculated and a four-node shell element was used to model the specimens. The numerical results are shown in Table 35 in conjunction with the experimental results. For the samples with core thicknesses of 3 mm (0.12 in.) and 6.35 mm (0.25 in.), the experimental failure loads are consistently higher than the numerical linear buckling loads. This can be explained by friction in the experimental boundary fixtures. The friction caused the actual experimental boundary conditions to be less than ideal freely rotating end conditions, which caused the experimental results to be higher than the numerical results. The numerical results were therefore normalized to the no-hole case and are summarized in Table 36 in conjunction with the normalized experimental results. For the samples with a core thickness of 12.70 mm (0.5 in.), the higher loads overcame the friction and the end fixtures behaved more like simply supported boundary conditions. Therefore the numerical results agreed with the experimental results.

The friction at the end support can be modeled by moments applied at the boundaries as shown in Figure 54. The Governing Equation is

$$\frac{d^2v}{dx^2} + k^2v = -\frac{1}{EI} M_o \quad \dots\dots\dots (1)$$

where

$$k = \sqrt{\frac{P}{EI}} \quad \dots\dots\dots (2)$$

The deflection equation is

$$v = -\frac{M_o}{P} \frac{(\cos \sqrt{\frac{P}{EI}} L - 1)}{\sin \sqrt{\frac{P}{EI}} L} \sin \sqrt{\frac{P}{EI}} x + \frac{M_o}{P} (\cos \sqrt{\frac{P}{EI}} x - 1) \quad \dots\dots\dots (3)$$

The Solution for the shear force V is

$$V = \frac{M_o k}{\cos \frac{kL}{2}} \sin \left(\frac{kL}{2} - kx \right) \quad \dots\dots\dots (4)$$

Algebraic rearrangement of this expression results in the equation given in reference 7.

Shear force V is a maximum when

$$\frac{kL}{2} - kx = \frac{\pi}{2} \quad \dots\dots\dots (5)$$

Solving for x

$$x = \frac{L}{2} \left(1 - \sqrt{\frac{P_{cr}}{P}} \right) \dots\dots\dots (6)$$

Where P is the failure load and P_{cr} is the Euler buckling load.

$$P_{cr} = \frac{\pi^2 EI}{L^2} \dots\dots\dots (7)$$

The sample with a core thickness of 3 mm (0.12 in.) has a failure load of 3.47 KN and a Euler buckling load of 1.29 KN. For this sample the analysis yields $x = 0.2L$. The sample with a core thickness of 6.35 mm (0.25 in.) has a failure load of 6.32 KN and a Euler buckling load of 4.18 KN. For this sample the analysis yields $x = 0.1L$. The experimental results for these two samples show good correlation to the predicted failure locations.

Continuing to solve for the bending moment M

$$M = \frac{M_o}{\cos \frac{kL}{2}} \cos \left(kx - \frac{kL}{2} \right) \dots\dots\dots (8)$$

The maximum bending moment occurs at

$$x = \frac{L}{2} \dots\dots\dots (9)$$

Examination of the experimental samples shows that failure at the hole is due to bending while failure at the quarter point away from the hole is due to foam core shear failure. A geometric non-linear stress analysis using an eight-node layered shell element was conducted to take a closer look at the stresses within the different composite layers to support the experimental findings. The analysis shows that a sample without a hole subjected to a given compressive load has a greater foam core shear stress at the quarter point than at the center. With a hole at the center, the foam core shear stress at the quarter point increases as the hole diameter increases. However, the carbon skin bending stress at the hole increases at a faster rate than the foam core shear stress. When the hole diameter reaches a critical diameter, the bending stress at the hole becomes more critical in failure than the core shear stress at the quarter point. As a result, the failure mode changes from foam core shear failure at the quarter point to skin bending failure at the hole. Figure 55 shows the rate of increase for both stresses with increasing hole diameter. With a 6.35 mm (0.25 in.) hole, the sample fails at the quarter point due to foam core shear failure. With a 12.70 mm (0.5 in.) hole, the bending stress at the hole is more critical than the core shear stress at the quarter point and the sample fails at the hole. Between these two points, the failure mode makes a transition from foam core shear failure at the quarter point to bending failure at the hole. Further refinement of the transition location is a recommended area for further study.

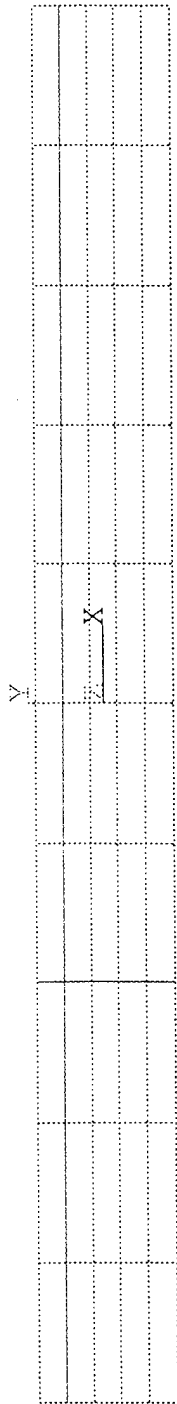


Figure 49. Finite Element Mesh for the No-Hole Case.

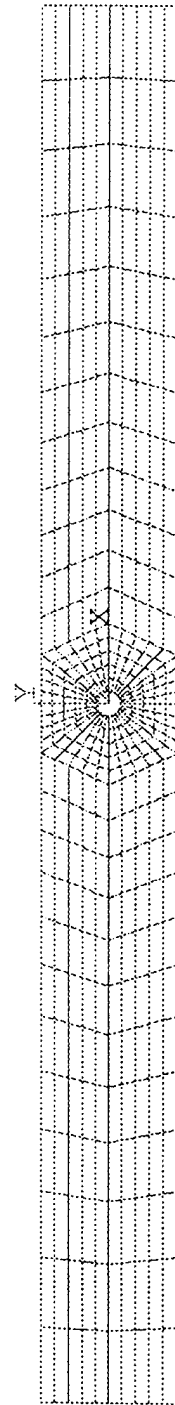


Figure 50. Finite Element Mesh for the Center Hole Case.

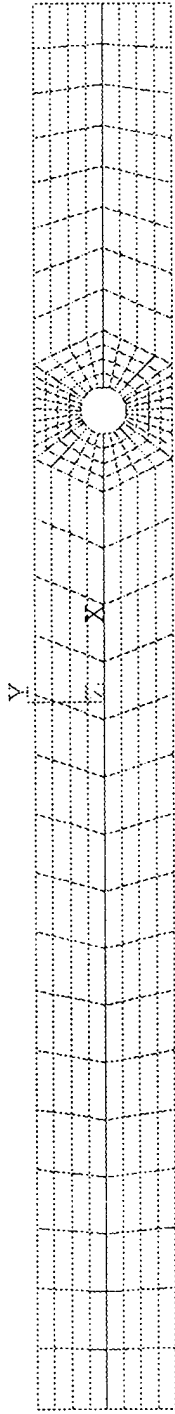


Figure 51. Finite Element Mesh for the Quarter Point Hole Case.

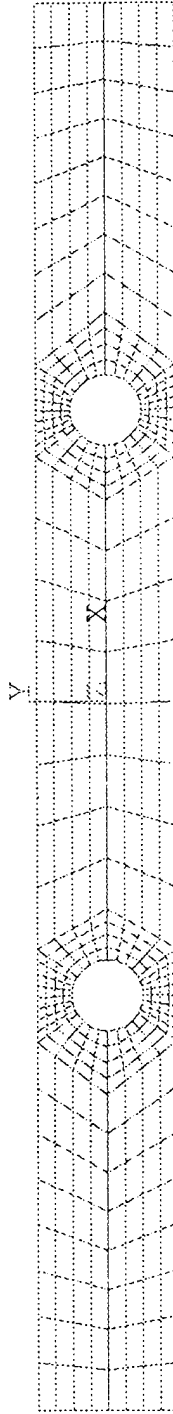


Figure 52. Finite Element Mesh for the Case with a Hole at Each Quarter Point.

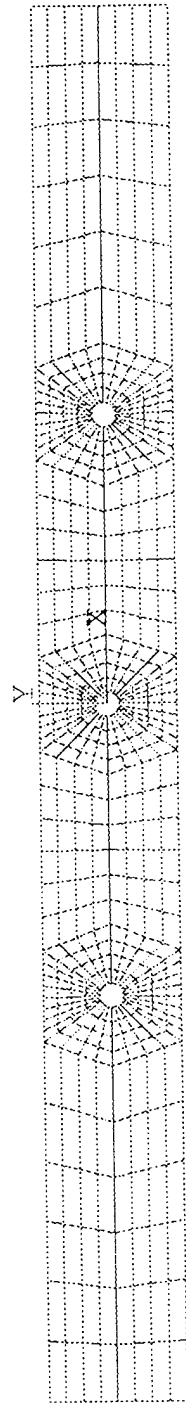


Figure 53. Finite Element Mesh for the Case with Holes at Both Quarter Points and at the Center.

Key: Experimental Numerical	3 mm thick foam	6.35 mm thick foam	12.70 mm thick foam
no hole	3.47 KN at qtr pt 1.29 KN	6.32 KN at qtr pt 4.18 KN	14.23 KN at qtr pt 14.31 KN
6.35mm hole at the center	1.27 KN	4.14 KN	12.31 KN at qtr pt 14.18 KN
12.70 mm hole at the center	2.74 KN at qtr pt 1.24 KN	6.13 KN at qtr pt 4.04 KN	10.23 KN at center 13.86 KN
19.05 mm hole at the center	1.16 KN	5.24 KN at center 3.82 KN	10.28 KN at center 13.17 KN
22.23 mm hole at the center	2.61 KN at center 1.12 KN	3.67 KN	12.65 KN
6.35 mm hole at one quarter point	1.27 KN	4.15 KN	13.41 KN at qtr pt 14.24 KN
6.35 mm hole at both quarter points	1.27 KN	4.13 KN	13.21 KN at qtr pt 14.17 KN
6.35 mm hole at both quarter points and at center	1.26 KN	4.10 KN	13.15 KN at qtr pt 14.16 KN
12.70 mm hole at both quarter points	1.20 KN	5.74 KN at qtr pt 4.01 KN	13.78 KN
19.05 mm hole at both quarter points	1.13 KN	4.99 KN at qtr pt 3.74 KN	12.91 KN

Table 35. Numerical and Experimental Result.

Key: Experimental Numerical	3 mm thick foam	6.35 mm thick foam	12.70 mm thick foam
no hole	1.0 at qtr pt 1.0	1.0 at qtr pt 1.0	1.0 at qtr pt 1.0
6.35mm hole at the center	0.99	0.99	0.87 at qtr pt 0.99
12.70 mm hole at the center	0.79 at qtr pt 0.97	0.97 at qtr pt 0.97	0.72 at center 0.97
19.05 mm hole at the center	0.91	0.83 at center 0.91	0.72 at center 0.92
22.23 mm hole at the center	0.75 at center 0.87	0.88	0.88
6.35 mm hole at one quarter point	0.99	0.99	0.94 at qtr pt 0.99
6.35 mm hole at both quarter points	0.99	0.99	0.93 at qtr pt 0.99
6.35 mm hole at both quarter points and at center	0.98	0.98	0.92 at qtr pt 0.99
12.70 mm hole at both quarter points	0.96	0.91 at qtr pt 0.96	0.96
19.05 mm hole at both quarter points	0.89	0.79 at qtr pt 0.90	0.90

Table 36. Normalized Experimental and Numerical Results.

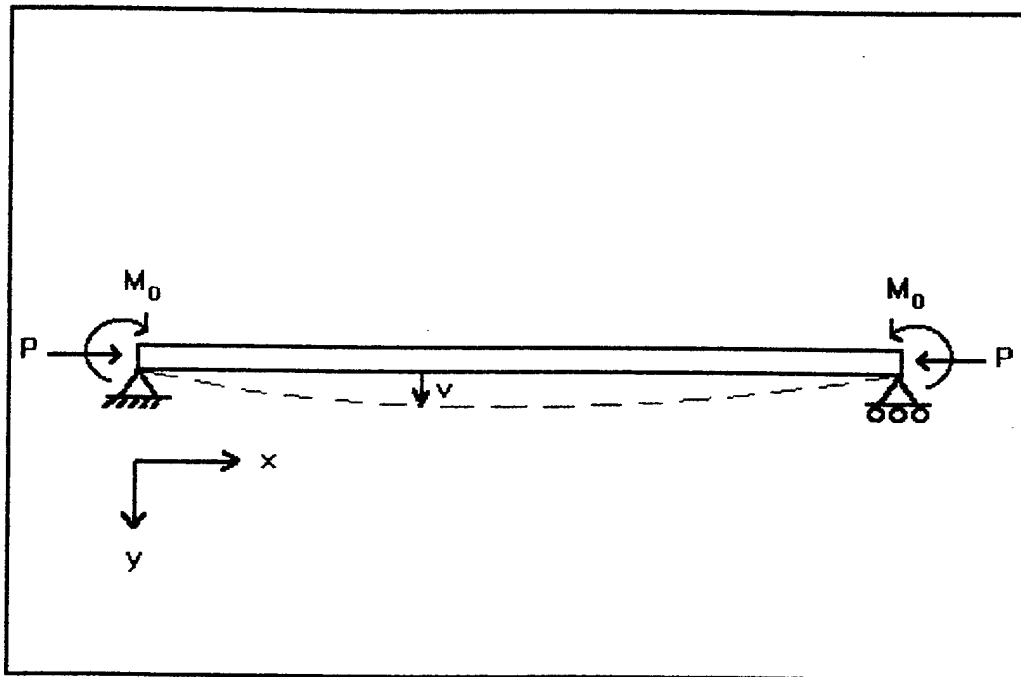


Figure 54. End fixture friction model.

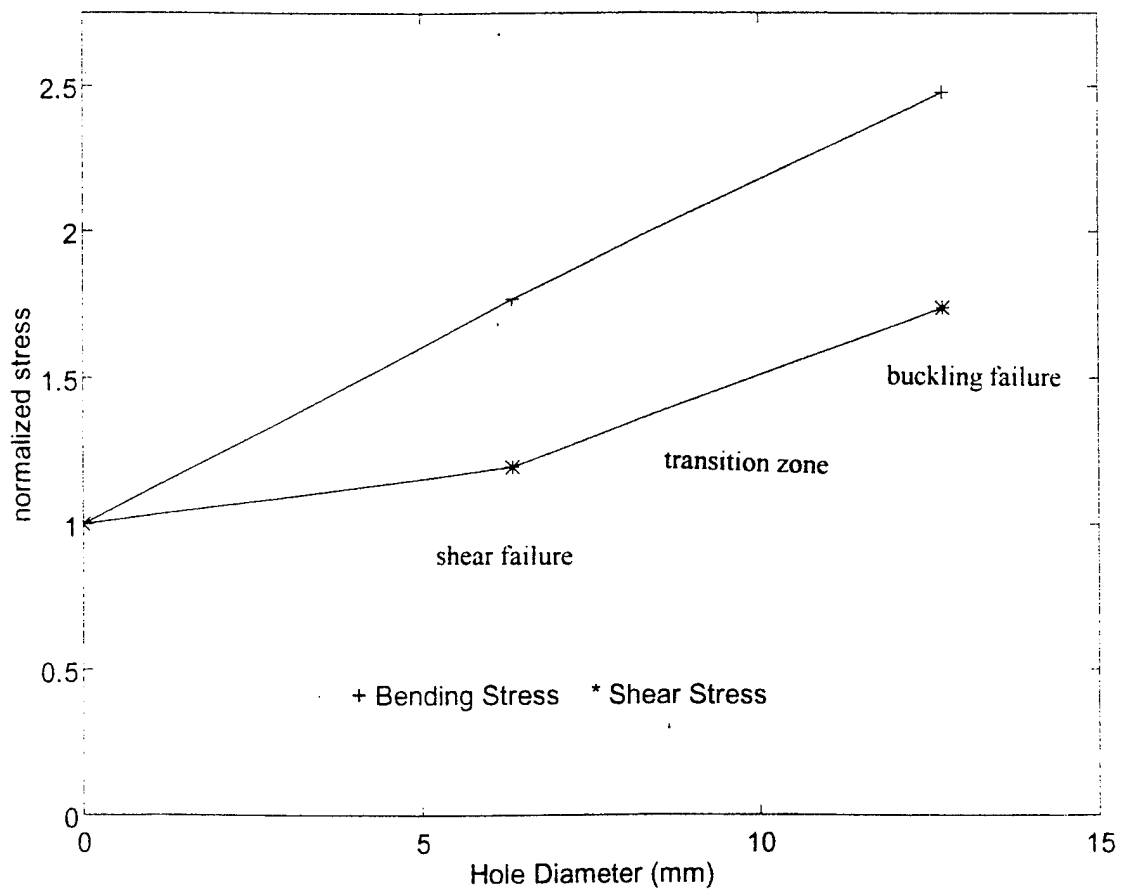


Figure 55. Normalized stresses vs. Hole Diameter.

VIII. CONCLUSIONS AND RECOMMENDATIONS

Four-point bending is not an effective test method to evaluate the effects of stress concentration at a hole in a foam cored sandwich composite beam as foam core shear failure occurs at a support point prior to bending failure at the hole.

A foam cored sandwich composite beam loaded in compression has a greater foam core shear stress between the end support and the quarter point than at the center and fails between the end support and the quarter point by foam core shear failure. With a hole at the center, the foam core shear stress at the quarter point increases as the hole diameter increases. However, the carbon skin bending stress at the hole increases at a faster rate than the foam core shear stress. When the hole diameter reaches a critical diameter, the bending stress at the hole becomes more critical in failure than the core shear stress at the quarter point. As a result, the failure mode changes from foam core shear failure at the quarter point to skin bending failure at the hole. The critical diameter decreases as the foam core thickness increases. Sandwich composites with a thick core are most commonly used in practical applications. When thick core composites are used, the critical diameter is small and failure is by bending.

The experimental compression failure loads are higher than the numerical linear buckling loads for samples with core thicknesses of 3 mm (0.12 in.) and 6.35 mm (0.25 in.). This can be explained by friction in the experimental boundary fixtures. The friction at the end supports can be modeled by moments applied at the boundaries. As derived in Chapter

VII, the failure location can be calculated.

An area of future study is the interaction of holes and delamination during the failure process. It is recommended that simply-supported experimental boundary fixtures with low friction be developed.

LIST OF REFERENCES

1. Lingaiah, K., and Suryanarayana, B.G., "Strength and Stiffness of Sandwich Beams in Bending", *Experimental Mechanics*, vol. 31, pp. 1-7, March 1991.
2. Clawson, L.A., "Experimental Study of Delaminated Sandwich Composite Subject to Impact and/or Compression Loading", Naval Postgraduate School Thesis, June 1995.
3. Prasad, C.B., and Shuart, M.J., "Moment Distributions Around Holes in Symmetric Composite Laminates Subjected to Bending Moments", *AIAA Journal*, vol. 28, no. 5, pp. 877-882, May 1990.
4. Ueng, E.S., and Lin, J.K., "Stress Concentrations in Composite Laminates", *Journal of Engineering Mechanics*, vol. 113, pp. 1181-93, August 1987.
5. Meyer, E.S., and Dharani, L.R., "Stress Concentration at Circular Cutouts in Buffer Strip Laminates", *AIAA Journal*, vol. 29, no. 11, pp. 1967-72, November 1991.
6. France, P.J., and Cloud, G.L., "Strain-Relief Inserts for Composite Fasteners- An Experimental Study", *Journal of Composite Materials*, vol. 26, no. 5, pp. 751-768, 1992.
7. Timoshenko, S.P., and Gere, J.M., *Theory of Elastic Stability*, McGraw-Hill, 1961.

INITIAL DISTRIBUTION LIST

No. Copies

1. Defense Technical Information Center.....2
 Cameron Station
 Alexandria, Virginia 22304-6145

2. Library, Code 013.....2
 Naval Postgraduate School
 Monterey, California 93943-5101

3. Department Chairman, Code ME.....1
 Department of Mechanical Engineering
 Naval Postgraduate School
 Monterey, California 93943-5000

4. Curriculum Officer, Code 34.....1
 Department of Mechanical Engineering
 Naval Postgraduate School
 Monterey, California 93943-5000

5. Professor Y. W. Kwon, Code ME/KW.....2
 Department of Mechanical Engineering
 Naval Postgraduate School
 Monterey, California 93943-5000

6. Commandant, (G-MTH-2).....2
 United States Coast Guard
 2100 Second St. S.W.
 Washington, D.C. 20593-0001

7. LT Peter J. Sistare, USCG.....2
 U.S. Coast Guard Marine Safety Center
 400 7th St. S.W.
 Washington, D.C. 20590-0001